
A Review of Quasi-Coherent Structures in a Numerically Simulated Turbulent Boundary Layer

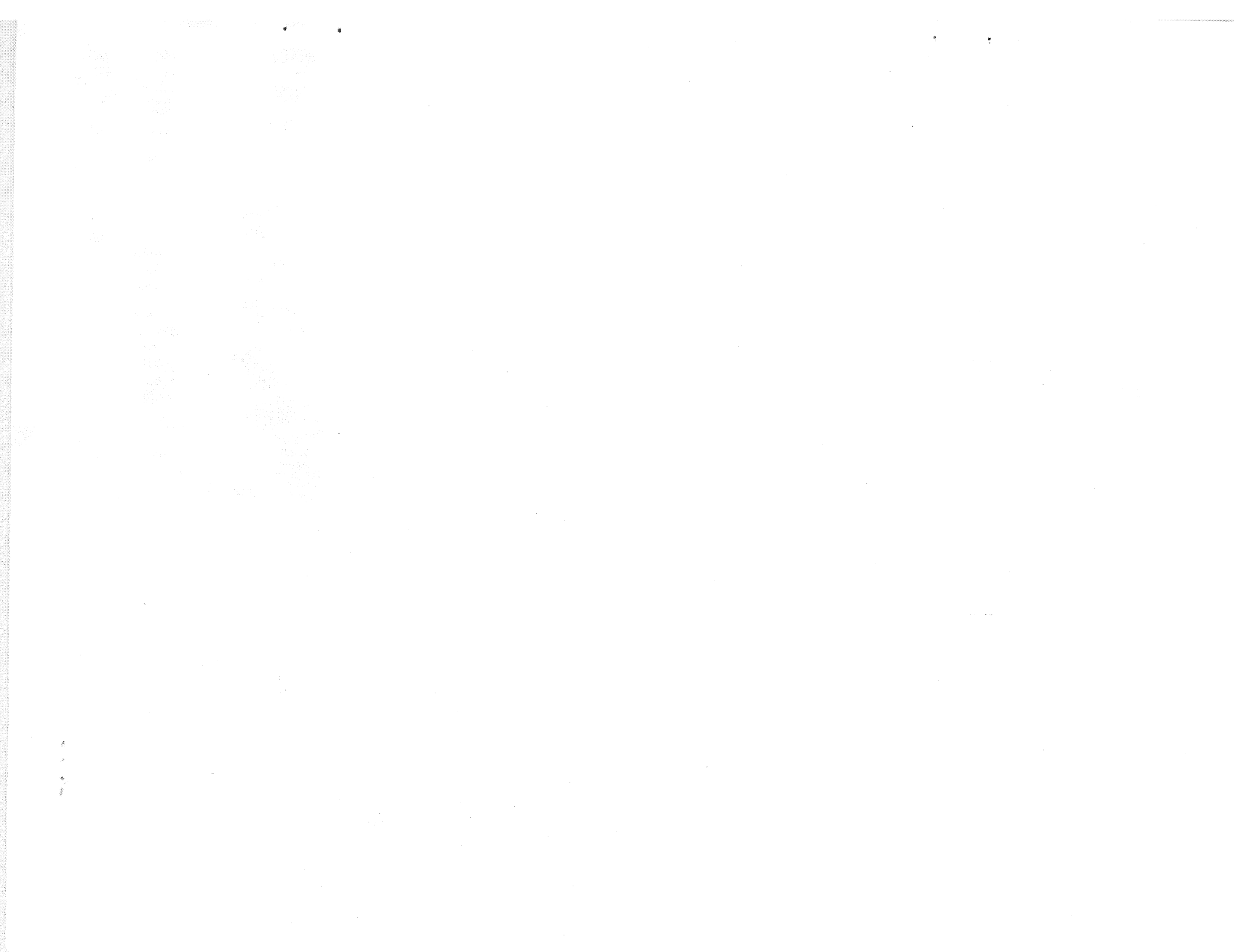
S. K. Robinson, Ames Research Center, Moffett Field, California
S. J. Kline, Stanford University, Stanford, California
P. R. Spalart, Ames Research Center, Moffett Field, California.

May 1989

NASA

National Aeronautics and
Space Administration

Ames Research Center
Moffett Field, California 94035



A REVIEW OF QUASI-COHERENT STRUCTURES IN A NUMERICALLY SIMULATED TURBULENT BOUNDARY LAYER

S. K. Robinson, S. J. Kline,¹ and P. R. Spalart

Ames Research Center

SUMMARY

This paper presents preliminary results of a comprehensive study of the structural aspects of a numerically simulated number turbulent boundary layer. A direct Navier-Stokes simulation of a flat-plate, zero pressure gradient boundary layer at $Re_\theta = 670$ was used. Most of the known nonrandom, coherent features of turbulent boundary layers are confirmed in the simulation, and several new aspects of their spatial character are reported. The spatial relationships between many of the various structures are described, forming the basis for a more complete kinematical picture of boundary layer physics than has been previously known. In particular, the importance of vortex structures of various forms to the generation of Reynolds shear stress is investigated.

INTRODUCTION

In spite of decades of experimental research, the structure of turbulent boundary layers, and the dynamical processes by which turbulence is created and maintained in boundary layers are only partially understood. The incomplete nature of our understanding has prevented the results of turbulence structure research from making any significant contributions to either predictive modeling schemes or to turbulence control methodologies.

This continuing situation has given rise to a novel approach to the problem: a community-wide re-evaluation of the knowledge. In simple terms, the aim is to develop a clear picture of what we know with certainty and to form a "strategic plan" for attacking the voids in our knowledge. The eventual goal is to lay the foundation for a class of "statistical-structural" models for turbulent boundary layers. The new and critical element of this effort is the involvement of the research community. A detailed description of the process and status of the cooperative evaluation project is given in Kline and Robinson (1988).

The limitations of experimental methods for unravelling the puzzle of turbulence physics are well understood but are, to a large degree, inherent. Fixed probes at a small number of points in space can be weak tools for determining the characteristics of three-dimensional structures that exhibit large

¹Stanford University, Stanford, CA 94305.

variations in time and space. Although many groups agree that simultaneous use of flow-visualization and probe arrays are optimum, it remains difficult to resolve Eulerian probe-based quantitative data with visual information from markers in a three-dimensional unsteady flow-field. It is to the credit of the researchers in the field that so much has been learned about the structure of turbulence through experimentation.

To complement the large volume of experimental results in the field, this companion study of the cooperative project is designed to take advantage of the direct Navier-Stokes turbulence simulation databases available at NASA Ames. Although the simulations are currently limited to simple geometries at low Reynolds numbers, there are many advantages to studying turbulence structure numerically, as discussed later in this paper, and also by Moin (1984).

Community involvement also plays a fundamental role in the study of the numerical simulation data. As the major unknowns are identified through the cooperative evaluation work, their resolution can be pursued in the simulations. The questions and suggestions of the participants in the cooperative project have helped pose the critical questions for study via the numerical simulation databases. This paper will present an overview of the recent results of this approach.

The objective of the current effort is to combine the many known structural elements and events with new insight gained from the numerical studies, to form a complete dynamical picture of flat-plate boundary layer turbulence, at least for low Reynolds numbers. This picture should include information on: (1) the spatial character of each class of structure; (2) the spatial relationships between different structures; (3) the generation and evolution of structures; (4) the statistical relevance of each class of structure; and (5) descriptions of the dominant sequences of events that are responsible for maintaining turbulence.

An additional goal is to investigate the effects of Reynolds number on boundary layer structural features, at least over the limited range of Reynolds numbers available in the simulations. A final important objective is to simulate a variety of experimental techniques in the databases to improve and possibly extend the understanding gained from experimental results.

In the remainder of this paper, a brief description of Spalart's boundary layer simulation will be given as will an outline of the strategy we are employing to study the database. A preliminary taxonomy of structures is presented, and examples of each class are illustrated and described. Finally, several samples of spatial relationships between structures will be shown. The results confirm a number of published experimental findings and also present new information on the structure of turbulent boundary layers.

Since the results of this work are voluminous and are still in progress, conclusions concerning time-evolutions of structural features will be deferred to a subsequent paper. The results presented herein are meant to serve as an introduction to the character of turbulence structure in the simulated boundary layer.

This project is jointly funded by NASA Ames Research Center, The Air Force Office of Scientific Research, and The Office of Naval Research.

All of the computational work has been done at NASA Ames. The simulation code was written and run by Philippe Spalart at Ames. The core of the graphical display software was developed by P. Buning of Ames, and by F. Merritt and G. Bancroft of Sterling Software. Support for this project has

been provided by the personnel and equipment of the Ames Workstation Applications Office and the Imaging Technology Branch, and by the Experimental Fluid Dynamics Branch, of which S. K. Robinson is a member.

The time of Prof. S. J. Kline and of O. Manickham and L. Portela is supported by AFOSR and ONR.

Useful discussions of this work have been provided by Dr. J. Kim at Ames, by Professors P. Moin and B. Cantwell at Stanford, and by the many participants of the cooperative program in turbulence structure. Reviews of this paper were provided by Prof. J. Wallace at University of Maryland, by Prof. R. Brodkey at the Ohio State University, and by L. Portela of Stanford University.

ADVANTAGES/DISADVANTAGES OF THE USE OF FULL SIMULATION DATABASES FOR THE STUDY OF TURBULENCE STRUCTURE

The central advantage of the numerical simulations over experimental investigation is that in the databases, we can collect a large sample of structural features first, and then decide what statistics are pertinent to compute. In the laboratory, the process is usually reversed. The flow can be made visible, but quantitative structural information from probes must be somehow extracted by clever statistical analysis of the data. This method is necessarily incomplete, and has proven to be seriously misleading in some cases. The averaging and filtering inherent in most statistical techniques can discard phase information, disguise true characteristics of individual realizations, create false symmetries, and contaminate ensemble averages by the inadvertent inclusion of extraneous flow elements. The current availability of numerical turbulence marks the first time in history that a sufficient sample of each structure can be inspected a priori and then quantitative statistics gathered for the significant features.

In addition to this subtle, but crucial point, the full simulation results offer a number of other more obvious, but important advantages:

1. Selected structural features can be pursued both forward and backward in time, and this process can be iteratively refined.
2. All structures of a given type that exist in the computational domain can be made simultaneously visible, allowing evaluation of case-to-case variations.
3. The spatial relationships between the several types of co-existing structures can be studied.
4. Structural features that are virtually unmeasurable in the lab can be displayed (e.g., low-pressure cores of unsteady vortices).
5. By combining time evolution with the ability to display different types of structures simultaneously, it becomes possible to examine the spatio-temporal relationships among the various elements of the dominant structures.
6. Rapid turnaround time of structural queries and the availability of specific frozen data volumes and time-sequences allow iterative reprocessing.

The structural aspects of the direct numerical simulation databases have been studied in depth for some years by their authors (e.g., Kim, 1985; Kim and Moin, 1986; Moser and Moin, 1987; Moin and Spalart, 1988). Recently, experimentalists (including the first two authors of this paper) have begun to explore the simulations as "numerical wind tunnels" to confirm and extend experimental results, and to help design future experiments. Participation by turbulence structure experimentalists in the 1987 Summer Program at the NASA/Stanford Center for Turbulence Research resulted in a number of significant findings from investigations of the numerical databases.

The direct Navier-Stokes simulation work is still in its infancy, and has several limitations. These include high costs in time and dollars (both for the simulation itself and for the later analyses), and restriction to low Reynolds numbers, simple geometries, and periodic boundary conditions. Nevertheless, the study of the simple flows now available will not only enlighten us about those exemplary cases, but will also aid in establishing appropriate procedures for application to the more complex flows of the future.

NUMERICAL SIMULATION SPECIFICATIONS

Spalart's direct Navier-Stokes numerical simulation of a flat-plate turbulent boundary layer (Spalart, 1988) has been chosen as the initial simulation database to explore. The code has been run to statistical equilibrium for four Reynolds numbers, $Re_\theta = 225, 300, 670,$ and 1410 . Most of the analysis so far has utilized the $Re_\theta = 670$ case, due to the high computational cost of the $Re_\theta = 1410$ case. At $Re_\theta = 670$, each time-step is computed on a $384 \times 288 \times 85$ grid, comprising 9.4 million nodes. At each node, for each time-step, pressure and all three components of velocity (and thus vorticity) are available. Grid resolution is 12.8 viscous lengths in the streamwise (x) direction, and 4.3 viscous lengths in the spanwise (z) direction. Resolution in the wall-normal (y) direction varies from 0.03 to 16.0 viscous lengths, with 14 grid points between the wall and $y^+ = 10$. The grid spacing for the $Re_\theta = 670$ case gives a computational domain with streamwise, spanwise, and wall-normal dimensions of 4900, 2500, and 1100 viscous units, respectively (fig. 1). The boundary layer is approximately 300 viscous units thick at this Reynolds number. Further details concerning the computational method and the results are given in Spalart (1988).

The simulation provides access to a turbulent region approximately 25 wall-streak spacings wide and 16 boundary layer thicknesses long. The velocity and pressure field of the computation has been saved on tape for 104 time steps, each three viscous time-units apart. This database offers a massive amount of information with high resolution in both space and time. Estimates suggest the amount of data available will provide sufficient sample sizes for spatial statistics of the major structural features.

A subvolume of the total computational domain is shown in figure 2. In the wall-normal (y) direction, the subvolume reaches from $y^+ = 3$ to $y^+ = 250$, which is approximately 80% of the mean boundary layer thickness. Over 1600 subvolumes of this size are available in the stored turbulence database. For comparison purposes, the same subvolume of data (referred to as "subvolume S") will be used repeatedly to illustrate several structural features. Many other subvolumes are being included in the overall analysis, however, so the figures presented here should be considered examples, and not necessarily representative of all realizations. It is worth noting that examples of each class of structural feature are detectable in nearly every subvolume studied so far.

Spalart (1988) has performed a number of statistical checks of the numerical boundary layer, which generally show good agreement with available experimental results. These include turbulence intensities, skewnesses, flatness factors, Reynolds stress and turbulence kinetic energy budgets, and spectra. The most significant known discrepancy is a 5% overprediction of the friction coefficient for the highest Reynolds number case. In addition, near-wall fourth-order statistics, especially for v' , show a dependence on grid resolution. It is unclear how significant these may be in terms of the structural behavior of the turbulence. Results of our analyses so far indicate that the simulation is structurally indistinguishable from a physical low Reynolds number boundary layer.

ANALYSIS STRATEGY

The problem at hand is to understand the physics of turbulence creation and maintenance in boundary layers. Spalart's numerical simulation offers access to over 31 gigabytes of flow-field data. The computational and graphical power available to study the simulation results makes possible the pursuit of hundreds of "interesting" questions. Effective progress toward an understanding of turbulence production therefore demands a well thought-out strategy in order to set work priorities.

We have adopted the following six-phase strategy for the study of the simulation databases (fig. 3):

- I. (a) Identify structures in the numerical boundary layer that are known to exist in laboratory boundary layers. These can be grouped into eight classes, which are delineated in the next section.
(b) Once examples of these structures have been identified in the simulation results, obtain detailed descriptions of their spatial character by studying individual time-steps.
- II. Determine the spatial relationships between the various structures by visualizing them together in individual "frozen" time steps.
- III. Study the spatio-temporal relationships between structures by using all the stored time-steps and, where necessary, computing intermediate solutions at very small time increments ($\Delta t^+ = 0.3$) between the stored time-steps.
- IV. Determine the statistical significance of the various structures, their apparent generation mechanisms and any interaction events. Populations, frequencies in space and time, and statistics of occurrence will be computed. Contributions to future statistical/structural models will be made at this stage by computing probability distributions of events and structures, and their contributions to specific terms in the Reynolds-averaged model equations.
- V. Combine the results of stages I through V to develop a phenomenological model of the maintenance of turbulence in flat-plate boundary layers. This should include a description of the important sequences of events, and should describe the roles of all classes of experimentally observed structure. The flow of cause and effect within these sequences should be modeled, as well as any significant interactions between structural features.

VI. Simulate various experimental techniques, including multi-sensor probes and convected visual markers.

Phases I through IV involve only the kinematics and statistics of turbulence structure. As J. M. Wallace has reminded us, a picture of the dynamics does not emerge from passive observation of phenomena. Some kind of model must be proposed which links observed sequential events with causative mechanisms. Thus, only Phase V directly addresses the problem of dynamics in the turbulent boundary layer.

In the context of this strategy, most quantitative experimental results have addressed Phases I, II, and IV, while most flow-visualization studies could be categorized as Phase III. A number of authors have proposed structural models which include dynamical hypotheses and so belong in Phase V. Our Phase V work will involve testing the many models published by the community in the simulated turbulence, with the goal of combining the best parts of each into a single, and hopefully more complete, phenomenological model.

Phase VI of the strategy involves the simulation of various probe-based and visual experimental methods. In the numerical simulation, spatial variations can be considered separately from temporal variations. This may lead to clarification of probe-based results, which are generally Eulerian and hence treat space and time as a single, inherently combined variable.

The six-phase analysis strategy allows us to build up knowledge in a logical order, and facilitates prioritization of the large number of possible queries that might otherwise become disorderly and overwhelming. In the current study, the phases of the strategy represent an iterative, rather than a one-pass, sequential process. So far, work has been done under all six phases, but none have been completed. As noted, the current paper focuses largely upon results of Phases I and II of the research program.

TAXONOMY OF STRUCTURES

A consistent and accepted definition of “structure” (in the turbulence sense) has not yet surfaced. Thus, it may be viewed as a hopeless task to categorize the many flavors of turbulence structure to be found in the literature. However, a taxonomy, even though somewhat arbitrary, can help focus thinking and inject organization into the somewhat tangled mass of information on the subject.

Therefore, we have divided the various structures, events, flow modules, and organized motions found in the literature into eight classes. The intent is to include all types of non-random events that have been singled out for study by the researchers in the field, rather than utilize a definition that would necessarily exclude some of the data. This classification is only one of several possibilities, and the following list is not a conclusion of the current work, but rather a starting point for it.

A Classification of Boundary Layer Turbulence Structures:

- (1) Wall low-speed streaks
- (2) Ejections of low-speed fluid outward from the wall

- (3) Sweeps of high-speed fluid inward toward the wall
- (4) Vortical structures of various forms
- (5) Near-wall shear layers, exhibiting strong spanwise vorticity and du'/dx
- (6) Near-wall "pockets," seen as regions swept clean of near-wall marked fluid in experiments
- (7) Large (delta-scale) discontinuities in the streamwise velocity, or "backs"
- (8) Large (delta-scale) motions capped by bulges in the outer turbulent/potential interface

Kline and Robinson (1988) give descriptions and some of the known characteristics for each of these structural classes.

The present classification is meant to provide a skeleton of organization on which the study of the numerical simulations can build. Reflected in the broad coverage of the list is the objective of including all of the known structural features of turbulence in the current study, rather than just a few. Thus the categorization is comprehensive if not final.

PHASES I AND II: EXAMPLES OF THE SPATIAL CHARACTER OF EACH STRUCTURAL CLASS AND SELECTED SPATIAL RELATIONSHIPS

Sublayer Streaky Structure

Figure 5 shows an instantaneous plan view of the x - z plane at $y^+ = 2$ in the simulated turbulent boundary layer. The low-speed regions (streamwise velocity less than the local mean) are elongated and thin, in agreement with many experimental observations. (Here and elsewhere in the paper, "local mean" refers to the spatial average over the entire computational x - z plane at constant y^+ , for at least five time steps.) Streamwise coherence of single low-speed streaks often exceeds 1500 viscous lengths, with widths ranging from 20 to 80 Δz^+ . The streaky character of the instantaneous low-speed regions is somewhat more pronounced than shown by marked fluid in laboratory flows. This is because markers in low-speed streaks often lift away from the wall during ejections, leaving the remaining near-wall streak unmarked and invisible. However, the current results appear consistent with the wall-temperature data of Hirata and Kasagi (1979) in which continuous visualization at the wall was achieved using liquid crystals.

The high-speed regions in the sublayer (fig. 5) are considerably less elongated and somewhat wider than the low-speed regions. Streamwise lengths of high-speed regions seldom exceed 800 x^+ , and widths range from 40 to 110 Δz^+ . This difference in "streakiness" is to be expected, since high-speed fluid generally originates from outside the sublayer where the mean velocity gradient is lower and the flow is known to be less streak-like. Experimental flow visualizations have not shown the character of high-speed regions clearly, however, since fluid markers introduced near the wall collect in the low-speed regions. Since high-speed regions in the sublayer are less elongated than the low-speed regions, the term "high-speed streaks" is not used in the current study.

Another characteristic of low-speed streaks is shown in figure 6, which is an instantaneous plan-view of the boundary layer at $y^+ = 15$. The colored contours mark regions of significant value of the products $(-u')(+w')$ and $(-u')(-w')$. This product serves as a “streak-turning” parameter, since it highlights low-speed streaks $(-u')$ that simultaneously exhibit spanwise motion $(\pm w')$. This correlation may be termed $u'w'_2$ and $u'w'_3$, after the quadrants it occupies in the $u'w'$ hodograph plane. It was noticed by one of the authors and J. Swearingen that $u'w'_2$ and $u'w'_3$ contours display a vaguely “cross-hatched” pattern, suggestive of possible transverse propagation mechanisms near the wall. Swearingen et al. (1987) have drawn parallels between this behavior and spanwise oscillations related to breakdown instabilities in curved-wall flows. In the simulated boundary layer, significant near-wall spanwise velocities are commonly associated with “leg” or “neck” vortices (see below). A complete explanation for the spanwise motions of the low-speed streaks awaits further investigation.

Ejections

The quadrant technique will be used to define and identify ejections, or regions of low streamwise velocity with motion outward from the wall. The quadrant method involves splitting the instantaneous product of u' and v' into four categories according to the quadrant occupied in the $u'v'$ hodograph. Since its introduction by Wallace et al. (1972) and by Willmarth and Lu (1972), the quadrant method has been widely used to assign structural significance to motions that contribute to the boundary layer closure term, the Reynolds shear stress.

It is important to distinguish between the Reynolds shear stress $-\overline{u'v'}$, which is defined only as an average, and the instantaneous value of $u'v'$. To facilitate this distinction, the new term “shear product” will be used to refer to the instantaneous value of $u'v'$ at a location in space.

Figure 4 shows the four quadrants into which the shear product can be split, and the names associated with their respective motions (Wallace et al., 1972). The contributors to the positive Reynolds shear stress are quadrants 2 and 4. The concepts of ejection and sweep imply a coherent movement of fluid, rather than the occurrence of quadrant 2 or 4 motion at a single point in space. In the current work, ejections are arbitrarily defined as instantaneous regions of quadrant 2 shear product that extend at least ten viscous lengths in any direction. Sweeps are defined similarly. Thus, every ejection is a quadrant 2 motion, but not necessarily vice versa. Note that under this definition, sweeps and ejections may occur anywhere in the boundary layer.

Figure 7 shows contour surfaces of quadrant 2 shear product in the instantaneous computational sub-volume, S . For the figure, the contour value was set to detect strong quadrant 2 motions, with $u'v'_2$ equal to $4u\tau^2$. This and many other realizations show that strong ejections occur with two types of instantaneous spatial character: 1) thin and elongated in the buffer and lower log regions, and 2) broader and more blob-like in the outer log and wake regions. The spanwise extent of the outer-region ejections ranges up to $\Delta z^+ = 200$. Since ejections near the wall originate from low-speed streaks by definition, their character is expected to be at least somewhat elongated. Ejections are not observed to extend over the entire streamwise length of a streak, however. Only portions of the low-speed regions extend out of the sublayer.

Sweeps

Sweeps are regions in which the shear product $u'v'$ occupies the fourth quadrant in the $u'v'$ plane (fig. 4). Instantaneous contour surfaces of quadrant 4 shear product in the subvolume S are shown in figure 8. The contour threshold is the same as for figure 7; that is, the iso-surfaces correspond to

quadrant 4 shear product equal to $4u_\tau^2$. At any given time, strong sweeps occupy less volume in the simulated boundary layer than equally strong ejections. This spatial result agrees with the probe-based statistics of Wallace et al. (1972), Willmarth and Lu (1972), and others, who have shown ejections to dominate the contributions to the Reynolds shear stress outside the buffer region. The spatial character of high-speed fluid with a wallward velocity component is somewhat different than that of ejections. Strong sweeps are only occasionally elongated in the streamwise direction, and tend to have spanwise dimensions of less than $100 \Delta z^+$, regardless of distance from the wall.

Low-Speed Streaks with Ejections and Sweeps

Figure 9 is a plan-view of an x - z plane in the simulated boundary layer at $y^+ = 15$. Ejections and sweeps are shown for the same contour levels as listed above. Low-speed streaks are identified by contours of streamwise velocity $3u_\tau$ below the local mean. Strong ejections are seen to occur only on low-speed streaks, as they must by definition (both are regions of $-u'$). The simulated boundary layer is seen to agree with Corino and Brodkey's (1969) and Bogard and Tiederman's (1986) finding that several ejections may arise from a single low-speed streak, although the number of ejections per streak is dependent upon the contour levels chosen for $-u'$ and $u'v'^2$. The contour value for second quadrant $u'v'$ in figure 9 corresponds to a value of approximately 2.6, when normalized by the product of $u'(\text{rms})$ and $v'(\text{rms})$ at $y^+ = 15$. Strong ejections seem to originate from the central portion of streaks more often than from either end.

As expected from experimental results and from previous simulations (Moin, 1984), the contours of strong quadrant 2 and 4 motions are highly intermittent in space; neither displays the extended streamwise coherence of the low-speed regions, although quadrant 2 motions are somewhat elongated in the x -direction. The spanwise scale of sweeps is slightly larger than the low-speed streaks and the ejections, but their extent is still less than $80 z^+$. Thus, sweep motions in the buffer zone are narrow and localized, rather than broad intrushes.

When strong ejections and sweeps are found in close proximity at a given time, they are often laterally associated, in a side-by-side pair. This characteristic was also noted by Moin (1984) in simulated turbulent channel flow, and is evident in figure 9. Sweeps and ejections virtually never follow each other closely in the streamwise direction, contrary to several published structural models. However, slight skewing of the sweep/ejection pair in the x - z plane would cause a fixed probe to detect one followed closely in time by the other. Most single-point conditional sampling schemes do not allow for spanwise variations, so ensemble averages that show sweeps following ejections are to be expected, but are misleading if interpreted via Taylor's hypothesis, with the additional assumption that the motion lacks significant spanwise component.

The lateral pairing of vertical motions near the wall is more clearly shown in figure 10, in which instantaneous contours of v' are plotted for the x - z plane at $y^+ = 15$. Figure 10 shows that outward motions ($+v'$) nearly always occur closely beside inward vertical motions ($-v'$). This was also noted by Moin (1984) in channel flow simulations. This character suggests that in the buffer region, the occurrence of strong outward motion is strongly associated with an occurrence of wallward motion. The spanwise dimensions of significant wallward motions are limited to less than approximately 70 viscous lengths. The pattern in figure 10 is highly suggestive of localized, quasi-streamwise vortical motions, which have been discussed in a number of publications (Bakewell and Lumley, 1967; H. T. Kim et al., 1971; Blackwelder and Eckelman, 1979; Smith and Schwartz, 1983). The spanwise dimensions of the $\pm v'$ pairs range from 40 to 70 viscous lengths. The streamwise extent of the pairs ranges from 50 to 250 viscous lengths; however, this is not indicative of the streamwise dimensions of near-wall

quasi-streamwise vortices. Since the figure depicts a plane of data at constant y , a vortex with an inclination angle to the wall would be intersected in a limited region by the plane. Note that laterally arranged triplets of alternating positive and negative v' , which suggest the occurrence of vortex pairs, are relatively uncommon, but do exist. Most significant vertical motion in the buffer region appears to be associated with single vortices.

Vortical Structures

For the current work, vortical structures are defined as identifiable vortices, usually with segments of varying orientation in space. Under this definition, regions of significant vorticity do not necessarily qualify as vortical structures. The problem that arises from any reference to vortices is the definition of a vortex in unsteady viscous flow. In the cross-stream (y - z) plane of a zero pressure-gradient boundary layer, the time-averaged flow is nearly zero. In this plane, a working definition of a vortex is as follows: A vortex exists when instantaneous streamlines mapped onto the cross-stream plane display a roughly circular or spiral pattern; the core of this vortex will be oriented substantially streamwise. In any plane with significant mean motion, this definition becomes ambiguous due to the necessary choice of a reference frame velocity. From a reference frame moving with the core of the vortex, this same definition should hold, although it requires identifying the vortex core before defining the vortex itself. Thus, the above definition of a vortex is useful as a check of other vortex-identification methods, but not as an a priori tool in any plane other than the cross-stream (y - z) plane.

Distinction must be made, of course, between vortices and vorticity. Since regions of strong vorticity are not uniquely associated with vortices, the spatial character of the vorticity field in the turbulent boundary layer tends to be noisy and inconclusive with respect to vortical structures. This is demonstrated in figure 11, in which iso-surfaces of the three fluctuating components of vorticity in subvolume S are shown. Clearly, understanding of vortical structures requires a technique for marking only instantaneous vortices in the turbulent flow field.

Vortex lines have been used extensively by Kim and Moin (1986) to study the structure of vortices in a numerically simulated turbulent channel flow. This method, however, requires some meaningful criteria with which to choose starting locations for the vortex line tracing. In addition, vortex lines do not reflect the local strength of vorticity, so that dense bundles that occur in regions of very low vorticity could attract undue attention. Finally, although vortex lines must move with the fluid particles (neglecting viscosity) during time evolution, vortices, which are bunched sections of vortex lines, need not. Thus the method of vortex lines can be arbitrary and inconclusive unless coupled with an independent means of identifying vortex locations.

Near-wall vortices with mostly streamwise orientation have been the subject of a number of experimental investigations (Praturi and Brodkey, 1978; Blackwelder and Eckelman, 1979; Smith and Schwartz, 1983; Swearingen and Blackwelder, 1987). By taking a cross-stream cut through the simulated boundary layer and plotting velocity vectors or streamlines, such vortical motions are easily found with the above definition of a vortex. Figure 12 shows an instantaneous cut through a low-speed streak and its neighboring high-speed region in subvolume S . Velocity vectors in the cross-plane (v' - w') clearly meet the criteria of roughly circular streamlines and so a trial vortex has been identified in the data.

A method is required to trace the instantaneous, three-dimensional extent of vortical structures in space. Our proposal is to utilize the fact that vortex cores should be regions of low pressure. In figure 13, low-pressure and cross-plane velocity vectors are plotted for the same instantaneous plane of data as shown in figure 12. Fluctuating pressure is shown in color in figure 13, with lighter shades

indicating lower pressure. The instantaneous $v'w'$ velocity vectors are overlaid as in figure 12. Marking the low pressure clearly identifies the vortex core in the example. In figure 13, the radial pressure gradient (normal to the core) is fairly large at the outer edge of the core, so the value of the pressure contour used to locate the vortex is not critical. A white contour line has been drawn in figure 13 for values of pressure equal to $4\rho u_\tau^2$ below the local mean. (Local mean refers to the average value at each y -location over the entire computational x - z plane, for several time-steps of the simulation.) For reference, the rms of the pressure fluctuations, normalized by ρu_τ^2 , varies from about 2.5 near the wall to 0.5 at the mean boundary layer edge (Spalart, 1988).

In three dimensions, contour lines become contour surfaces. The 3-D contour surface of constant low pressure that corresponds to the 2-D contour line in figure 13 is shown for subvolume S in figure 14. As can be seen in figure 14, low-pressure regions tend to be elongated and occur in a variety of shapes and sizes, apparently indicating a wide variation in the three-dimensional form of vortical structures. This observation is confirmed by the study of many other subvolumes in the database. Compared to the vorticity field shown in figure 11, the instantaneous pressure field of figure 14 is relatively noise-free, with a variety of structural features clearly evident. (Figures 11 and 14 display the same data set.) Comparison of figures 11 and 14 emphasizes the importance of distinguishing vortical structures from regions of concentrated vorticity.

The technique of marking low-pressure regions allows application of the vortex definition advanced earlier. The velocity of a candidate low-pressure region is first determined. Then the instantaneous streamlines in a plane normal to the axis of elongation of the low-pressure zone are computed from a frame of reference moving with the low-pressure region. Roughly circular or spiral streamlines confirm the existence of a vortex.

It is not immediately clear whether a discernible low-pressure region is both a necessary and a sufficient condition for the existence of a vortex in the flow field. Many cuts normal to the axes of elongated low-pressure regions have been made. In every case so far, the velocity vectors in a cut-plane moving with the mean velocity of the low-pressure region has displayed roughly circular or spiral instantaneous streamlines. Although most low-pressure regions are elongated, there are several convoluted volumes of low pressure that are globule-shaped. So far, the analyses show that virtually all elongated low-pressure regions are vortices. The non-elongated regions are not always identifiable as vortices, and are assumed to be due to other fluid interactions, such as local accelerations. Thus, the technique of mapping elongated low-pressure regions provides a means of identifying the instantaneous spatial extent of vortical structures in the simulation.

The loop-like vortical structures shown in figure 14 are strongly suggestive of the hairpin or horseshoe vortices discussed in many previous papers, beginning with Theodorsen (1952). To facilitate discussion of the vortical structure topology, various sections of the structures are labeled as follows: heads are vortices with mostly transverse orientation; necks are vortices that generally extend wallward and upstream from heads at an angle of approximately 45 degrees to the wall; legs are vortices with mostly streamwise orientation. Legs sometimes appear connected to and trailing from a head/neck vortical structure.

Although statistical compilations have not yet been completed, some preliminary statements may be made concerning the structural nature of the elongated low-pressure regions. First, arch- or horseshoe-like vortical structures (head/neck) combinations are common, but long leg vortices are not. The legs that do exist can be quite long in the streamwise direction, reaching up to at least $\Delta x^+ = 400$. True hairpin vortices, with two trailing legs, are very rare. Many vortical structures are strongly asymmetric.

Hook-like shapes, as in figure 14, appear relatively often. In some cases, the missing neck can be identified on an asymmetric hook-like vortical structure when the contour level of the isobaric surfaces is varied. Legs can be found without necks, and are seen both near the wall (center at $y^+ < 60$) and in the wake region. Vortical arches occur with a variety of scales, and their heads are found at y -locations ranging from the buffer region to the edge of the boundary layer. Arches are generally as tall (in the wall-normal direction) as they are wide. The spanwise extent of vortical arches ranges from 50 to 350 viscous lengths in the simulated layer. The above conclusions hold true over a range of $-p'$ contour values. In general, varying the $-p'$ contour level affects the diameter and, in some cases, the topological connectivity of the low-pressure regions, but does not significantly alter the overall form of the vortical structures marked by elongated regions of low pressure. A variety of statistics on the spatial character of vortical structures in the boundary layer will be reported in subsequent publications.

Vortices with Low-Speed Streaks, Sweeps, and Ejections

An example of the spatial relationship between low-pressure regions, low-speed regions, and quadrant 2 shear product is shown for the sample subvolume S in figure 15. Low-speed regions are identified by iso-surfaces of streamwise velocity $3u_\tau$ below the local mean. Surface contour values for uv_2 and pressure are the same as for figures 7 and 14, respectively. Portions of at least two elongated low-speed streaks are visible near the wall, as are significant regions of locally low-speed fluid away from the wall, both within and beyond the buffer zone. Figure 15 shows low-speed fluid concentrated below and upstream of the vortical heads, and alongside the trailing vortex leg. The arch-like vortical structures in the figure straddle elongated low-speed regions, similar to the manner described by Runstadler et al. (1963) and by Smith (1984). Just upstream of the smaller of the two vortical arches is a small transverse region of low pressure, which appears to be a newly formed secondary vortex, possibly rolled up on the low-speed fluid lifted by the action the downstream vortical arch in the manner described by Acarlar and Smith (1987). The formation of this particular secondary vortex is clearly visible in time evolutions of the simulation.

The regions where low-speed fluid possesses a significant outward velocity component are marked in red in figure 15 as quadrant 2 ejections. Most regions of lifting low-speed fluid are in close proximity to the isobaric surface.

The spatial relationship between low-pressure regions, strong ejections, and strong sweeps is shown for subvolume S in figures 16 (oblique view) and 17 (plan view). The instantaneous spatial association of both sweeps and ejections with the vortical structures is striking.

Strong ejection regions ($u'v'_2 \geq 4u_\tau^2$ in fig. 16) apparently occur in two locations: (1) Alongside quasi-streamwise leg vortices, on the inboard (towards the head) side of the leg. This is the upward-rotating side of the vortex, so the picture is kinematically consistent. (2) Underneath and upstream of a head vortex. Ejections in location 2 are significantly farther from the wall than those in location 1. Both the head and neck seem to contribute to the outward induction of low-speed fluid from upstream and below the head. Since leg vortices are relatively rarer than head/neck combinations, the majority of the strong ejections seem to be associated with the head/neck vortical structure.

For ejections along quasi-streamwise vortices, figure 17 clearly shows that a single vortex can be responsible for the lifting of low-speed fluid, in agreement with Pearson and Abernathy's (1984) numerical studies of vortices in viscous shear layers, and with the ensemble-averaged simulation results of Guezennec et al. (1987). This view differs from hairpin vortex models (e.g., Offen and Kline, 1975;

Smith, 1984) of the boundary layer, which have fluid lifting due to the combined action of a pair of counter-rotating quasi-streamwise vortices.

Strong sweeps are observed mainly in two locations: (1) On the outboard, wallward-rotating side of the leg vortex. Here, high-speed outer fluid is induced toward the wall in a sweep motion. (2) A wallward induction of high-speed fluid by the outboard side (away from the head) of a neck vortex. Sweeps are more common in location 2, since neck vortices are more common than leg vortices in the simulated boundary layer. In either case, sweeps are found to be closely related to the existence of vortical structures.

A large percentage of the Reynolds shear stress in the boundary layer is known to be produced by highly localized strong ejections and sweeps (e.g., H T. Kim et al., 1971; Brodkey et al., 1974; Willmarth, 1975). Visualizations of the simulated boundary layer (fig. 16 is an example) suggest that the generation of Reynolds shear stress is closely tied to the existence of coherent vortical structures. The conclusion that vortical structures are a critical element of turbulence production and momentum transfer in the boundary layer is in agreement with a number of previous experimental and numerical studies.

Near-Wall Shear Layers

The existence of sloping du/dy shear layers near the wall ($y^+ < 80$) of turbulent channels and boundary layers has been established both by flow-visualization studies (Corino and Brodkey, 1969) and by probe-based results (Kreplin and Eckelmann, 1979; Johansson et al. 1987a). The VITA technique in particular has been employed in a number of experimental studies to detect rapid changes in the streamwise velocity. Correlations of the experimental data have shown these velocity jumps to correspond to the passage of local shear layers with a steep downstream slope. Bogard and Tiederman (1987) have shown that such shear layers occur on the upstream face of an ejection from the buffer region, at the interface between the lifting low-speed fluid and the higher-speed fluid overtaking it from behind. The limited ability of the VITA technique to detect ejections implies that near-wall shear layers also occur in other locations. The origin and dynamical significance of these shear layers has remained poorly understood, however.

Recent work by Jimenez et al. (1987) in numerically simulated channel flows has shed new light on the role of near-wall shear layers. These authors have proposed a mechanism for the generation and maintenance of the shear layers which is essentially equivalent to that responsible for the instability of two-dimensional Tollmien-Schlichting waves.

Additional recent work on near-wall shear layers in numerically simulated turbulent flows has been reported by Johansson et al. (1987b). These authors found that shear layers in the near-wall region propagate with a velocity of about $10.6 u_\tau$, and retain their coherence over streamwise distances of 1000 viscous lengths. Johansson et al. also show that near-wall shear layers make important contributions to the conditionally averaged production of turbulent kinetic energy.

In the current study of the simulated boundary layer, the sublayer and buffer region are found to be well-populated with near-wall shear layers. Shear layers can be found in any randomly selected x - y slice through the data, and are most common below $y^+ = 80$. Several examples of near-wall shear layers in the simulation are shown in three unrelated side-views in figure 18. The structures are nearly parallel to the wall in the sublayer and slope at an increasing but shallow ($< 20^\circ$) angle farther from the wall.

The spanwise dimension of most near-wall shear layers ranges from 30 to 60 viscous lengths, implying that highly three-dimensional mechanisms are involved in their formation.

Near-Wall Shear Layers with Vortices and Ejections

A new observation made in the current study is that some of the near-wall shear layers roll up into transverse vortices. Transverse roll-up of internal shear layers has previously been observed outside the wall region ($y^+ > 200$) in experiments by Nychas et al. (1973). Figures 19 and 20 show an example of near-wall shear layer roll-up. In figure 19, the shear layer is visualized by contours of spanwise vorticity. Although the vorticity is high everywhere along the shear layer, a low-pressure region is seen to exist only at the outer tip, where a transverse vortex is indicated. The existence of a vortex at the tip of the shear layer is confirmed by the instantaneous vector field in figure 20, which has been plotted in a reference frame moving downstream with the shear layer tip at its propagation velocity of $15 u_\tau$. Observation of computed time-sequences confirms that the particular transverse vortex in figure 20 does appear after the formation of the shear layer.

Contours of quadrant 2 shear product show ejection-type contributions to the Reynolds shear stress in figure 19. A region of strong quadrant 2 motion is observed to be associated with the transverse roll-up of the shear layer, but is not present along the remainder of the shear layer. Although the dynamic relationship between near-wall shear layer roll-up and the ejection of low-speed streak fluid needs clarification, the current findings support the suggestion of several experimental studies (Acarlar and Smith, 1987; Swearingen and Blackwelder, 1987; Johansson et al., 1987a) that shear-layer instabilities in the wall region may play a major role in the production of turbulence.

High-Pressure "Potatoes" with Low-Pressure Vortical Structures

The simulation database presents opportunities not available in the laboratory, and this allows the study of an additional class of "structure," namely high-pressure regions. Figure 21 shows the high-pressure regions in the instantaneous subvolume S of the computation, and their spatial relationship to the low-pressure regions.

High- and low-pressure regions in the simulated boundary layer exhibit very different characters, as noted by Moin and Spalart (1988). Whereas the low-pressure regions tend to be elongated, the high-pressure regions are roundish and potato-shaped. These "pressure potatoes" often occupy the space just upstream of the head portions of arch-like vortical structures, and appear to exist at a convected local stagnation point which lies at the interface of high- and low-speed fluid. The dynamic consequences of the local convecting pressure gradient set up between the low-pressure vortex core and the following high-pressure region have yet to be fully explored.

Wall-Pressure Fluctuations

Contours of instantaneous wall-pressure fluctuations are shown for the simulated boundary layer in figure 22. The patterns are rounded rather than elongated, in agreement with experimental results (Dinkelacker et al., 1977) and previous simulations (Grötzbach and Schumann, 1979; Moin, 1984). High- and low-pressure regions appear similar in dimensions, with most regions ranging from 50 to 200 wall units in both directions. However, occasional high- and low-pressure regions with extents of over 400 viscous lengths occur. Although wall-pressure disturbances of this scale would be expected to be associated with events in the outer flow, their specific sources are unclear.

Pockets

When distributed markers are introduced into the sublayer of a turbulent boundary layer or channel, roughly circular regions devoid of marked fluid appear in the plan view. These have been named pockets (Falco, 1980a), and they give the visual impression of being a “footprint” of some outer structure that induces fluid toward the wall. Kim et al. (1987) have shown that pockets become visible in numerically simulated channel flow only with distributed fluid markers, not with simulated bubble-lines. This observation confirms a similar experimental finding of Falco. However, time evolution of the marked flow field is necessary to detect pockets with distributed markers. In the current analysis of the simulated boundary layer, we have endeavored to detect pockets in instantaneous flow fields.

If pockets are associated with wallward-moving fluid in the sublayer, the instantaneous streamlines in the x - z plane would be expected to diverge in the pocket region. Figure 23 shows instantaneous streamlines computed in the $y^+ = 2$ plane of the simulated boundary layer. Regions of abrupt spanwise divergence of the streamlines are evident in the figure. The spanwise dimensions of these regions are generally between 50 and 100 viscous lengths, in agreement with pocket dimensions reported by Falco (1983). A time evolution of simulated fluid markers is being performed by the authors to check whether the regions of streamline divergence in the numerical boundary layer are indeed pockets.

Pockets with Sweeps

Spanwise divergence of instantaneous streamlines in the sublayer is, by continuity and the streaky nature of the streamwise velocity in the sublayer, most likely to be associated with wallward velocity. Wallward fluid in the sublayer arrives from regions with relatively higher streamwise velocity, so diverging instantaneous streamlines are generally expected to be associated with uv_4 motions, or sweeps. Since sweeps are observed to be commonly associated with vortices in the simulated boundary layer, pockets may be the footprint of fluid swept toward the wall by vortical structures. Preliminary studies in the simulated data suggest that this reasoning is correct for at least some of the observed pockets. This idea is nominally consistent with Falco's (1980a) theory concerning pocket formation, although the form and motion of the responsible vortex remains in question.

In figure 23, regions of converging streamlines may be likened to “detachment” lines in a separating flow, and regions of diverging streamlines to “reattachment” lines. The figure shows that most “detachment” and “reattachment” lines lie at a significant angle to the mean (streamwise) velocity vector. Since near-wall $\pm v'$ motions have a strong association with quasi-streamwise vortical structures (legs), it appears that vortex legs are generally oriented at an angle to the mean flow in the x - z plane as well as in the x - y plane.

Pockets with Wall-Pressure Fluctuations

Figure 24 shows instantaneous streamlines at $y^+ = 2$ together with contours of instantaneous wall pressure. As expected, local regions of high pressure coincide with spanwise divergence of the streamlines (wallward motion) and low pressure regions occur along lines of converging streamlines (outward motion). (See also Moin and Spalart, 1988.) Thus, pockets may be expected to be evidence of local wallward motions above regions of high wall pressure.

Bulges in the Outer Interfaces/Large-Scale Motions

Kovasnay et al. (1970) and others have shown that the instantaneous outer interface between the turbulent boundary layer and the potential free stream consists of large-scale bulges, separated by deep, narrow incursions of free-stream flow into the layer. In the simulated boundary layer, the instantaneous edge of the rotational flow can be identified by contours of low total vorticity magnitude

$\left(\sqrt{\omega_x^2 + \omega_y^2 + \omega_z^2}\right)$, as shown in figure 25. The picture is essentially the same as given by Spalart (1988), and exhibits broad outward bulges and narrow irrotational incursions. The interface bulges have dimensions of the scale of the boundary layer thickness in both the streamwise (x) and transverse (z) directions. Figure 25 resembles visualizations of smoke-filled low Reynolds number boundary layers (e.g. Falco, 1980b).

The large-scale motion beneath bulges in the simulated boundary layer show a weak rotation in the direction of the mean shear, when observed from a frame of reference moving at $0.8 U_e$. This is in qualitative agreement with experimental findings for the large-scale motions (e.g., Blackwelder and Kovasznay, 1972; Falco, 1983).

Backs

Delta-scale, sloping structures with strong local values of du/dx have been investigated by a number of groups using multi-sensor temperature and velocity probes (e.g., Brown and Thomas, 1977; Chen and Blackwelder, 1978; Subramanian et al. 1982). Space-time correlations and conditional sampling procedures have given from 12 to 30 degrees for the outer-region angle between the wall and these large structures. Because these structures are commonly associated with the upstream side of the large-scale motions discussed above (Kovasznay et al., 1970), we will refer to them as "backs" (though some publications refer to them as "fronts").

At this time, we are drawing a distinction between "backs" (which also have transverse vorticity) and the previously discussed near-wall shear layers. Backs are tall (delta-scale) discontinuities in u , with limited (10-40 viscous lengths) streamwise thickness, and with spacing in the streamwise direction of the order of the boundary layer thickness. Near-wall shear layers have dimensions on the scale of the near-wall layer, and exist mostly below $y^+ = 80$. It is not yet clear if the size and spacing of these shear-layer structures are distributed smoothly from small to large, or if there is a bimodal distribution, suggesting two different types of structure. Recent statistical analyses of simulated turbulence by Moin et al. (1987) have shown some evidence of a "two-layer" structural makeup of a low Reynolds number channel. Experimental ensemble averages have not generally separated the data into two structures possibly because the commonly used VITA technique will trigger on either, independent of vertical scale. Also, the scale separation between the two structures, if such a separation exists, would be most pronounced at high Reynolds numbers, where probe sensors are usually too long to independently detect the small-scale structures near the wall. Recent multi-point detection techniques (e.g., Britz and Antonia, 1987; Fernando et al., 1987) should help clarify this point.

Following Thomas and Brown (1977), figure 27 shows instantaneous velocity vectors in an x-y plane moving at $0.8 U_e$ in the simulated boundary layer. A back structure is clearly evident as a large-scale, sloping shear layer with transverse vorticity. The picture is strikingly similar to Thomas and Brown's ensemble-averaged velocity field in the vicinity of backs. Figure 28 shows the instantaneous transverse vorticity associated with the back in figure 27.

Backs with Vortical Structures

Several researchers have reported on outer-flow vortical structures that are inclined to the wall downstream at approximately 45 degrees (e.g., Head and Bandyopadhyay, 1981; Kim and Moin, 1986). Hot-wire rake studies have consistently given from 12 to 30 degrees for the slope of the backs of large-scale motions in the outer region (Brown and Thomas, 1977; Rajagopalan and Antonia, 1979; Robinson, 1982). Bandyopadhyay (1980) attempted to resolve this discrepancy by speculating that the shallow-angle backs are composed of the heads of arrays of 45 degree hairpin vortices.

In the current work, an example of the spatial relationship between a back and a hook-like vortical structure is shown in figure 26. In this example, the back, which is sloped at about 30 degrees, is located upstream of the 45 degree vortical structure. Apparently, the low-speed fluid being left behind by the action of the vortex is crowded from behind by the faster upstream flow. The interface between the upstream fluid and the low-speed remnants of vortex induction forms the velocity discontinuity which is the back. In this scenario, the back is generated without need for the row of hairpin vortices suggested by Bandyopadhyay. Final conclusions on the relationships between backs, large-scale motions, and vortical structures will require the study of more examples, especially in the simulation at the higher Reynolds number, $Re_\theta = 1410$. The generality of the descriptions of the large scale motions in low Reynolds number simulations may be limited in view of Murlis et al.'s (1982) finding that the outer structure depends on viscosity up to $Re_\theta = 5000$.

CONCLUDING REMARKS

The current ongoing investigation of the quasi-coherent structures in a numerically simulated turbulent boundary layer has produced the following preliminary results:

1. Examples of all known classes of boundary layer structure have been identified in the simulated boundary layer.
2. High-speed regions in the sublayer are observed to be less elongated than the low-speed regions.
3. Low-pressure regions tend to be elongated, and apparently serve as a useful spatial detection method for instantaneous vortex cores.
4. Arch-like (head + neck) vortical structures with a broad range of sizes are common in the boundary layer, while quasi-streamwise vortices ("legs") with significant streamwise extent are relatively rare.
5. High-pressure regions are spheroid and rarely elongated, and typically occur just upstream and below the heads of vortical arches, at the interface between high- and low-speed regions.
6. There is a strong instantaneous spatial association between vortical structures and both ejections (uv_2) and sweeps (uv_4).

7. Both ejections and sweeps occur along quasi-streamwise "leg" vortices, but ejections are most common just upstream and below vortical arches. Sweeps occur most often on the outboard sides of the "necks" of vortical arches.

8. Some near-wall shear layers have been observed to roll up into transverse vortices, which are in turn associated with significant local contribution to the Reynolds shear stress through ejection (uv_2) motions. Shear layers not in the process of rolling up contribute only weakly to the Reynolds shear stress.

9. "Backs" of outer-region, large-scale motions have been identified in the simulation data. In some cases at least, the backs (at a characteristic angle of 18 to 30 degrees) are the interface between low-speed fluid trailing a single large-scale vortical structure and the following high-speed fluid.

Work on the spatio-temporal relationships between the various structures is under way, and results will be reported this year. Among the questions of primary focus are (1) the nature and importance of the interaction of the outer, large-scale motions with turbulence-producing events near the wall; and (2) the generation mechanisms and evolution histories of the common vortical structures. As noted, a variety of population and contribution statistics are being compiled to establish the statistical relevance of the observed structural features and interactions. Finally, simulated probes and visual markers are being applied to draw more direct comparisons between the simulated boundary layer and experimental observations.

The current work, along with the 1987 Center for Turbulence Research Summer Program, marks the opening of a new era in experimental fluid dynamics, in which full-simulation results are studied by experimentalists working in "numerical wind tunnels." The long-term benefits of this new activity should include 1) increased experimental emphasis on flows with more complex boundary conditions and higher Reynolds numbers, 2) development of advanced instrumentation with specialized measurement capabilities, 3) increased understanding of probe resolution, conditional averaging, and phase-jitter effects, and 4) joint experimental/numerical investigations of flows in which the two techniques are complementary.

It is hoped that the current study, as part of a community-wide assessment of the state of boundary layer structure knowledge, will accelerate progress toward a broad-based understanding of the dynamics of wall-layer turbulence.

REFERENCES

- Acarlar, M. S., and Smith, C. R., A Study of Hairpin Vortices in a Laminar Boundary Layer. Part 1: Hairpin Vortices Generated by a Hemisphere Protuberance, J. Fluid Mech., vol.175, p.1, 1987.
- Bakewell, H. P., Jr., and Lumley, J. L., Viscous Sublayer and Adjacent Wall Region in Turbulent Pipe Flow, Phys. Fluids, vol. 10, no. 9, p.1880, 1967.
- Bandyopadhyay, P., Large Structure with a Characteristic Upstream Interface in Turbulent Boundary Layers, Phys. Fluids, vol. 23, no. 11, p. 2326, 1980.
- Blackwelder, R. F., and Kovaszny, L. S. G., Time Scales and Correlations in a Turbulent Boundary Layer, Phys. Fluids, vol. 15, no.9, p.1545, 1972.
- Blackwelder, R. F., and H. Eckelmann, Streamwise Vortices Associated with the Bursting Phenomenon, J. Fluid Mech., vol. 94, part 3, p.577, 1979.
- Bogard, D. G., and Tiederman, W. G., Burst Detection with Single-Point Velocity Measurements, J. Fluid Mech., vol. 162, p.389, 1986.
- Bogard, D. G., and Tiederman, W. G., Characteristics of Ejections in Turbulent Channel Flow, J. Fluid Mech., vol. 179, p.1, 1987.
- Britz, D., and Antonia, R. A., A Computer Algorithm for the Identification of Temperature Fronts in a Turbulent Shear Flow, Exp. Fluids, vol. 5, p. 134, 1987.
- Brodkey, R. S., Wallace, J. M., and Eckelmann, H., Some Properties of Truncated Signals in Bounded Shear Flows, J. Fluid Mech., vol. 63, part 2, p. 209, 1974.
- Brown, G. L., and Thomas, A. S. W., Large Structure in a Turbulent Boundary Layer, Phys. Fluids, vol. 20, no. 10, part 2, p.5243, 1977.
- Chen, C. H. P., and Blackwelder, R. F., Large-Scale Motion in a Turbulent Boundary Layer: a Study Using Temperature Contamination, J. Fluid Mech., vol. 89, part 1, p.1, 1978.
- Corino, E. R., and Brodkey, R. S., A Visual Investigation of the Wall Region in Turbulent Flow, J. Fluid Mech., vol. 37, part 1, p.1, 1969.
- Dinkelacker, A., Hessel, M., Meier, G. E. A., and Schewe, G., Investigation of Pressure Fluctuation Beneath Turbulent Boundary Layer by Means of an Optical Method, Bericht, vol. 105, Max-Planck Institut fur Stromungsforschung, Gottingen, 1977.
- Falco, R. E., The Production of Turbulence Near a Wall, AIAA Paper 80-1356, 1980a.
- Falco, R. E., Combined Simultaneous Visualization/Hot-Wire Anemometry for the Study of Turbulent Flows, J. Fluid Mech., vol. 102, p.174, 1980b.

- Falco, R. E., New Results, a Review and Synthesis of the Mechanism of Turbulence Production in Boundary Layers and its Modification, AIAA Paper 83-0377, 1983.
- Fernando, E. M., Spina, E. F., Donovan, J. F., and Smits, A. J., Detection of Large-Scale Organized Motions in a Turbulent Boundary Layer, Proceedings of the 6th Symposium on Turbulent Shear Flows, Toulouse, France, September 7-9, 1987.
- Grötzbach, G., and Schumann, U., Direct Numerical Simulation of Turbulent Velocity, Pressure, and Temperature Fields in Channel Flows, in Turbulent Shear Flows I, F. Durst, B. E. Launder, F. W. Schmidt, and J. H. Whitelaw (Eds.), p. 370, Springer-Verlag, Berlin, 1979.
- Guezennec, Y. G., Piomelli, U., and Kim, J., Conditionally-Averaged Structures in Wall-Bounded Turbulent Flows, Proceedings of the Summer Program 1987, p. 263, Center for Turbulence Research, NASA/Stanford, 1987.
- Head, M. R., and Bandyopadhyay, P., New Aspects of Turbulent Boundary Layer Structure, J. Fluid Mech., vol. 107, p. 297, 1981.
- Hirata, M., and Kasagi, N., Studies of Large-Eddy Structures in Turbulent Shear Flows with the Aid of Flow-Visualization Techniques, Studies in Heat Transfer, J. P. Hartnett et al. (Eds.), Hemisphere, 1979.
- Jimenez, J., Moin, P., Moser, R. D., and Keefe, L. R., Ejection Mechanisms in the Sublayer of a Turbulent Channel, Proceedings of the Summer Program 1987, p. 37, Center for Turbulence Research, NASA/Stanford, 1987.
- Johansson, A. V., Alfredsson, P. H., and Eckelmann, H., On the Evolution of Shear-Layer Structures in Near-Wall Turbulence, in Advances in Turbulence, G. Comte-Bellot and J. Mathieu (Eds.), Springer-Verlag, 1987a.
- Johansson, A. V., Alfredsson, P. H., and Kim, J., Shear-Layer Structures in Near-Wall Turbulence, Proceedings of the Summer Program 1987, p.237, Center for Turbulence Research, NASA/Stanford, 1987b.
- Kim, H. T., Kline, S. J., and Reynolds, W. C., The Production of Turbulence Near a Smooth Wall in a Turbulent Boundary Layer, J. Fluid Mech., vol. 50, part 1, p.133, 1971.
- Kim, J., Turbulence Structures Associated with the Bursting Event, Phys. Fluids, vol. 28, no.1, p. 52, 1985.
- Kim, J., Overview of Research by the Turbulence Structure Group, Proceedings of the Summer Program 1987, p. 231, Center for Turbulence Research, NASA/Stanford, 1987.
- Kim, J., and Moin, P., The Structure of the Vorticity Field in Turbulent Channel Flow, Part 2. Study of Ensemble-Averaged Fields, J. Fluid Mech., vol. 162, p. 339, 1986.
- Kim, J., Moin, P., and Moser, R. D., Turbulence Statistics in Fully-Developed Channel Flow at Low Reynolds Number, J. Fluid Mech., vol. 177, p. 133, 1987.

- Kline, S. J., and Robinson, S. K., Quasi-Coherent Structures in the Turbulent Boundary Layer: Part I: Status Report on a Communitywide Summary of the Data, Zoran P. Zarić Memorial Seminar on Near-Wall Turbulence, Dubrovnik, Yugoslavia, May 16-20, 1988.
- Kovaszny, L. S. G., Kibens, V., and Blackwelder, R. F., Large-Scale Motion in the Intermittent Region of a Turbulent Boundary Layer, J. Fluid Mech., vol. 41, part 2, p.283, 1970.
- Kreplin, H.-P., and Eckelmann, H., Propagation of Perturbations in the Viscous Sublayer and Adjacent Wall Region, J. Fluid Mech., vol. 95, part 2, p. 305, 1979.
- Moin, P., Probing Turbulence via Large-Eddy Simulation, AIAA Paper 84-0174, 1984.
- Moin, P., and Spalart, P. R., Contributions of Numerical Simulation Data Bases to the Physics, Modeling, and Measurement of Turbulence in Recent Advances in Turbulence, R. E. Arndt and W. K. George (Eds.), Hemisphere Publishing Corp., Washington, D.C., 1988.
- Moin, P., Adrian, R. J., and Kim, J., Stochastic Estimation of Conditional Eddies in Turbulent Channel Flow. Proceedings of the 6th Symposium on Turbulent Shear Flows, Toulouse, France, September 7-9, 1987.
- Moser, R. D., and Moin, P., Direct Numerical Simulation of Curved Turbulent Channel Flow, NASA TM 85974. Also, J. Fluid Mech., vol. 175, p. 479, 1987.
- Murlis, J., Tsai, H. M., and Bradshaw, P., The Structure of Turbulent Boundary Layers at Low Reynolds Numbers, J. Fluid Mech., vol. 122, p.13, 1982.
- Nychas, S. G., Hershey, H. C., and Brodkey, R. S., A Visual Study of Turbulent Shear Flow, J. Fluid Mech., vol. 61, p. 513, 1973.
- Offen, G. R., and Kline, S. J., A Proposed Model of the Bursting Process in Turbulent Boundary Layers, J. Fluid Mech., vol. 70, part 2, p.209, 1975.
- Pearson, C. F., and Abernathy, F.H., Evolution of the Flow Field Associated with a Streamwise Diffusing vortex, J. Fluid Mech., vol.146, September, p. 271, 1984.
- Praturi, A. K., and Brodkey, R. S., A Stereoscopic Visual Study of Coherent Structures in Turbulent Shear Flow, J. Fluid Mech., vol.89, part 2, p. 251, 1978.
- Rajagopalan, S., and Antonia, R. A., Some Properties of the Large Structure in a Fully Developed Turbulent Duct Flow, Phys. Fluids, vol.22, no. 4, p. 614, 1979.
- Robinson, S. K., An Experimental Search for Near-Wall Boundary Conditions for Large Eddy Simulation, AIAA/ASME 3rd Joint Thermophysics, Fluids, Plasma and Heat Transfer Conference, St. Louis, Missouri, June 7-11, 1982.
- Runstadler, P. W., Kline, S. J., and Reynolds, W. C., An Experimental Investigation of the Flow Structures of the Turbulent Boundary Layer, Rept. MD-8, Thermosciences Div., Dept. Mech. Eng., Stanford Univ., 1963.

- Smith, C. R., A Synthesized Model of the Near-Wall Behavior in Turbulent Boundary Layers, in Proc. Eighth Symp. on Turbulence, Univ. Missouri-Rolla, 1984.
- Smith, C. R., and Schwartz, S. P., Observation of Streamwise Rotation in the Near-Wall Region of a Turbulent Boundary Layer, Phys. Fluids, vol. 26, no.3, p.641, 1983.
- Spalart, P. R., Direct Simulation of a Turbulent Boundary Layer up to $Re_\theta = 1410$, J. Fluid Mech., vol. 187, p. 61, 1988.
- Subramanian, C. S., Rajagopalan, S., Antonia, R. A., and Chambers, A. J., Comparison of Conditional Sampling and Averaging Techniques in a Turbulent Boundary Layer, J. Fluid Mech., vol. 123, p. 335, 1982.
- Swearingen, J. D., and Blackwelder, R. F., The Growth and Breakdown of Streamwise Vortices in the Presence of a Wall, J. Fluid Mech., vol.182, p. 255, 1987.
- Swearingen, J. D., Blackwelder, R. F., and Spalart, P. R., Inflectional Instabilities in the Wall Region of Bounded Turbulent Shear Flows, Proceedings of the Summer Program 1987, p. 291, Center for Turbulence Research, NASA/Stanford, 1987.
- Theodorsen, T., Mechanism of Turbulence, Proceedings 2nd Midwestern Conference on Fluid Mechanics, Ohio State Univ., Columbus, Ohio, 1952.
- Thomas, A. S. W., and Brown, G. L., Large Structure in a Turbulent Boundary Layer, 6th Australasian Hydraulics and Fluid Mechanics Conference, Adelaide, Australia, December 5-9, 1977.
- Wallace, J. M., Brodkey, R. S., and Eckelmann, H., Pattern-Recognized Structures in Bounded Turbulent Shear Flows, J. Fluid Mech., vol.83, part 4, p.673, 1977.
- Willmarth, W. W., Advances in Fluid Mechanics, vol. 15, p. 158, Acad., New York, 1975.
- Willmarth, W. W., and Lu, S. S., Structure of the Reynolds Stress Near the Wall, J. Fluid Mech., vol. 55, part 1, p. 65, 1972.

FIGURE CAPTIONS

Figure 1.– Computational domain.

Figure 2.– Strategy for structural analysis of numerical simulations.

Figure 3.– Computational subvolume.

Figure 4.– Quadrants of the $u'v'$ plane.

Figure 5.– Contours of fluctuating streamwise velocity in an x - z plane at $y^+ = 2$.
Blue to white: $u'^+ = +0.7$ to $+2.0$.
Red to yellow: $u'^+ = -0.7$ to -2.0 .

Figure 6.– Contours of $u'w'_2$ and $u'w'_3$ in an x - z plane at $y^+ = 15$.
Green to white: $u'w'_2/u_\tau^2 = 2.1$ to 14.9 .
Red to white: $u'w'_3/u_\tau^2 = -2.1$ to -14.9 .

Figure 7.– Quadrant 2 shear product in subvolume S.
Red: $u'v'_2/u_\tau^2 = -4.2$.

Figure 8.– Quadrant 4 shear product in subvolume S.
Blue: $u'v'_4/u_\tau^2 = -4.2$.

Figure 9.– Low-speed streaks, ejections, and sweeps in an x - z plane at $y^+ = 15$.
Yellow: $u'^+ = -3.0$.
Red: $u'v'_2/u_\tau^2 \leq -4.2$.
Blue: $u'v'_4/u_\tau^2 \leq -4.2$.

Figure 10.– Contours of $\pm v'$ in an x - z plane at $y^+ = 15$.
Magenta: $v'^+ = +1.0$.
Green: $v'^+ = -1.0$.

Figure 11.– Fluctuating vorticity in subvolume S (lowest y^+ shown is 28).
Yellow: $\omega_x'^+ = \pm 0$.
Red: $\omega_y'^+ = \pm 0$.
Blue: $\omega_z'^+ = \pm 0$.

Figure 12.– y - z plane cut through low/high-speed streak interface.
Yellow: $u'^+ = 0$ to -6.0 .
Blue: $u'^+ = 0$ to $+6.0$.
Green: instantaneous $v'w'$ vectors.

Figure 13.– y-z plane cut through low/high-speed streak interface.

Magenta to white: $p'^+ = 0$ to -12.0 .

White contour line: $p'^+ = -4.2$.

Green: instantaneous $v'w'$ vectors.

Figure 14.– Regions of low pressure in subvolume S.

White: $p'^+ = -4.2$.

Figure 15.– Regions of low pressure, low streamwise velocity, and quadrant 2 shear product in subvolume S.

White: $p'^+ = -4.2$.

Yellow: $u'^+ = -3.0$.

Red: $u'v'2/ u_{\tau}^2 = -4.2$.

Figure 16.– Regions of low pressure, quadrant 2 shear product, and quadrant 4 shear product in subvolume S.

White: $p'^+ = -4.2$.

Red: $u'v'2/ u_{\tau}^2 = -4.2$.

Blue: $u'v'4/ u_{\tau}^2 = -4.2$.

Figure 17.– Top view of Figure 16.

Figure 18.– Near-wall shear layers in an instantaneous x-y plane.

Blue to green: $\omega_z^+ = 0.2$ to 1.0 .

Figure 19.– Roll-up of near-wall shear layer.

Blue to green: $\omega_z^+ = +0.2$ to $+1.0$.

White: $p'^+ = -4.2$ to -17.0 .

Magenta to yellow: $u'v'2/ u_{\tau}^2 = -2.1$ to -12.8 .

Figure 20.– Roll-up of near-wall shear layer. Instantaneous uv velocity vectors in an x-y plane moving at $15u_{\tau}$.

Figure 21.– Regions of high and low pressure in subvolume S.

White: $p'^+ = -4.2$.

Green: $p'^+ = +4.2$.

Figure 22.– Instantaneous wall-pressure fluctuations.

Blue to green: $p_w^+ = +2.1$ to $+21.3$.

Magenta to white: $p_w^+ = -2.1$ to -21.3 .

Figure 23.– Instantaneous streamlines in an x-z plane at $y^+ = 2$.

Figure 24.— Instantaneous streamlines in an x-z plane at $y^+ = 2$, overlaid with contours of wall pressure.
Yellow to red: $p'^+ = +3.0$ to $+25.0$.
Blue to white: $p'^+ = -3.0$ to -25.0 .

Figure 25.— Contours of total vorticity magnitude in an x-y plane.
Blue to magenta: $|\omega^+| = 0.02$ to 1.0 .

Figure 26.— “Back” of large-scale motion with regions of low pressure in subvolume S.
White: $p'^+ = -4.2$.
Blue to magenta: $\omega_z = +0.2$ to $+3.0$.

Figure 27.— Instantaneous uv vectors in an x-y plane moving at $0.8 u_e$.

Figure 28.— Instantaneous transverse vorticity in same x-y plane as for Figure 27.
Blue to magenta: $\omega_z = +0.2$ to $+3.0$.

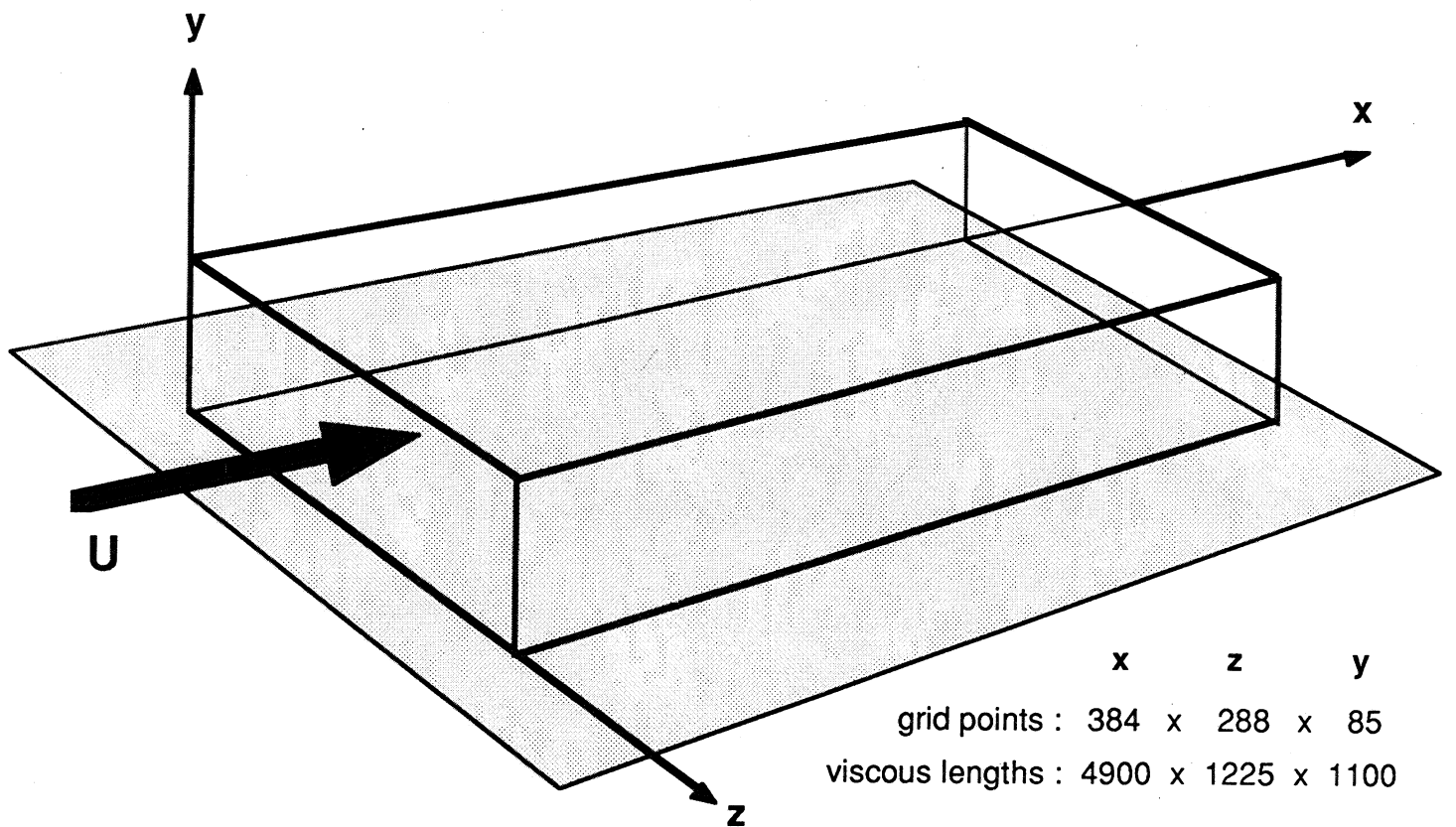


Fig. 1. Computational domain.

Part B - Numerical Simulation Analyses

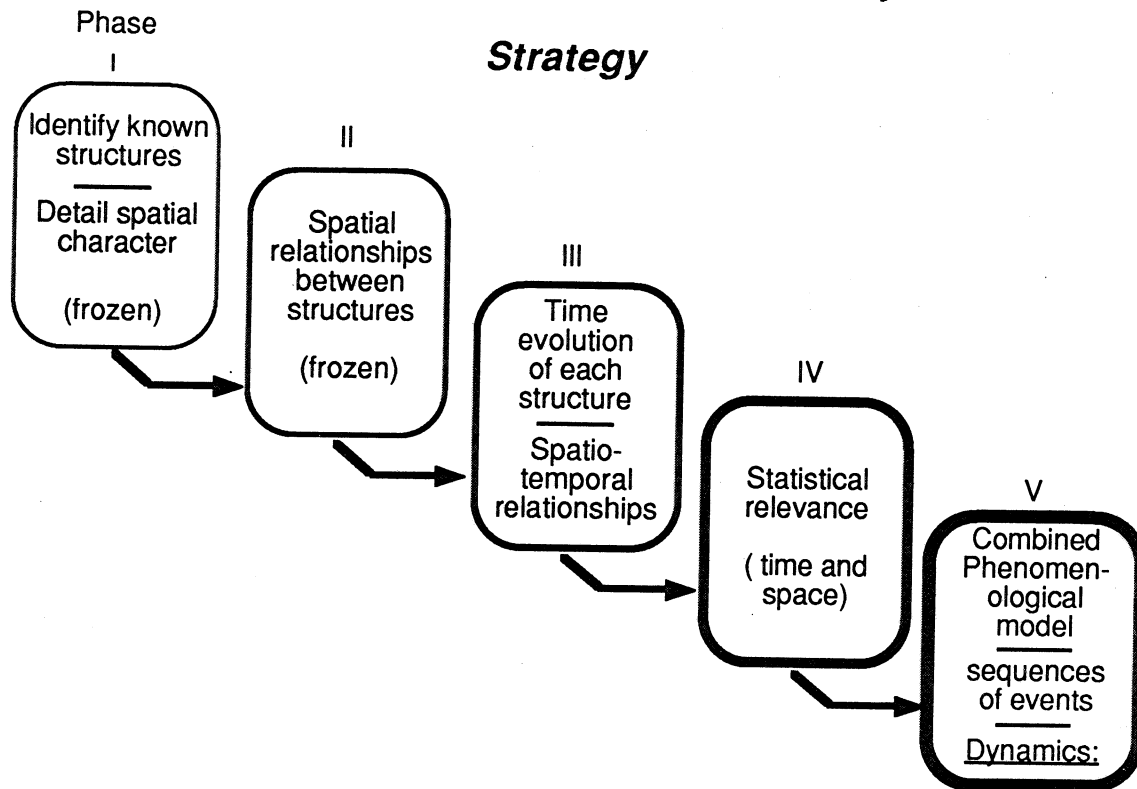


Fig. 2. Strategy for structural analysis of turbulence simulations.

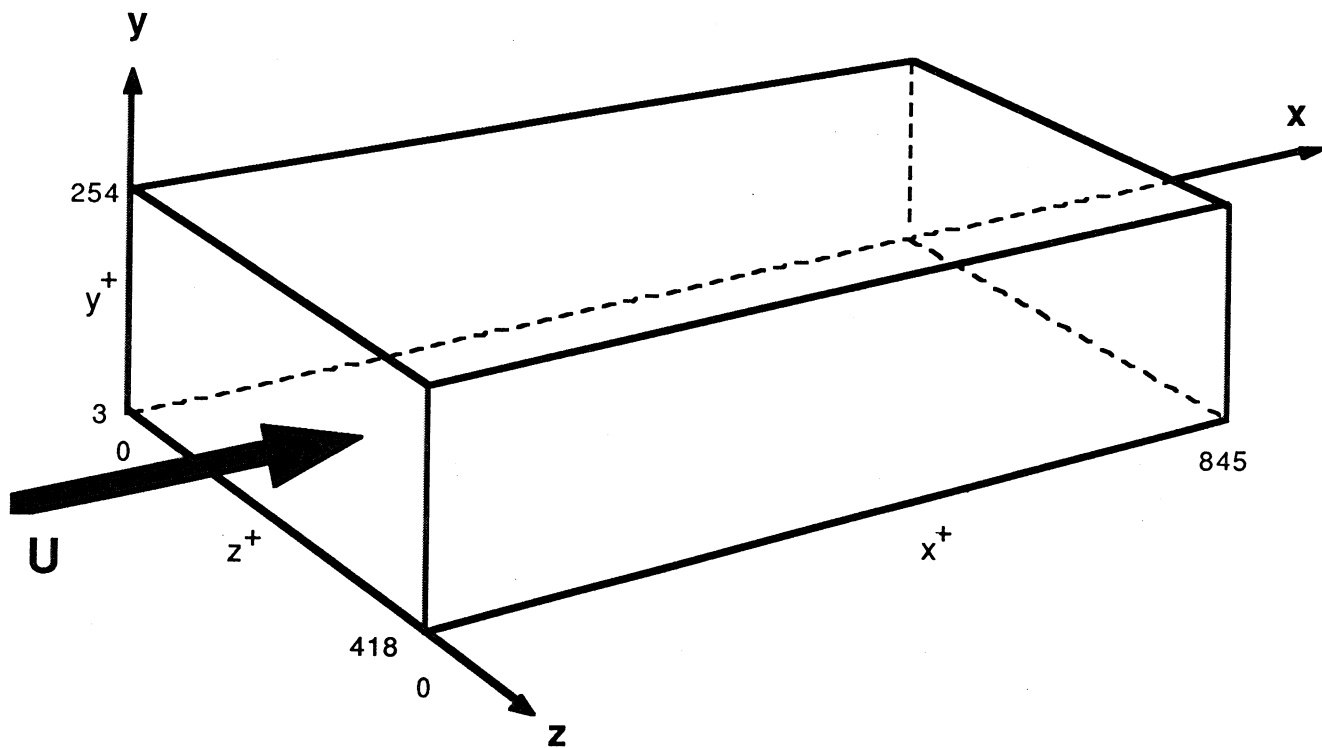


Fig. 3. Computational subvolume.

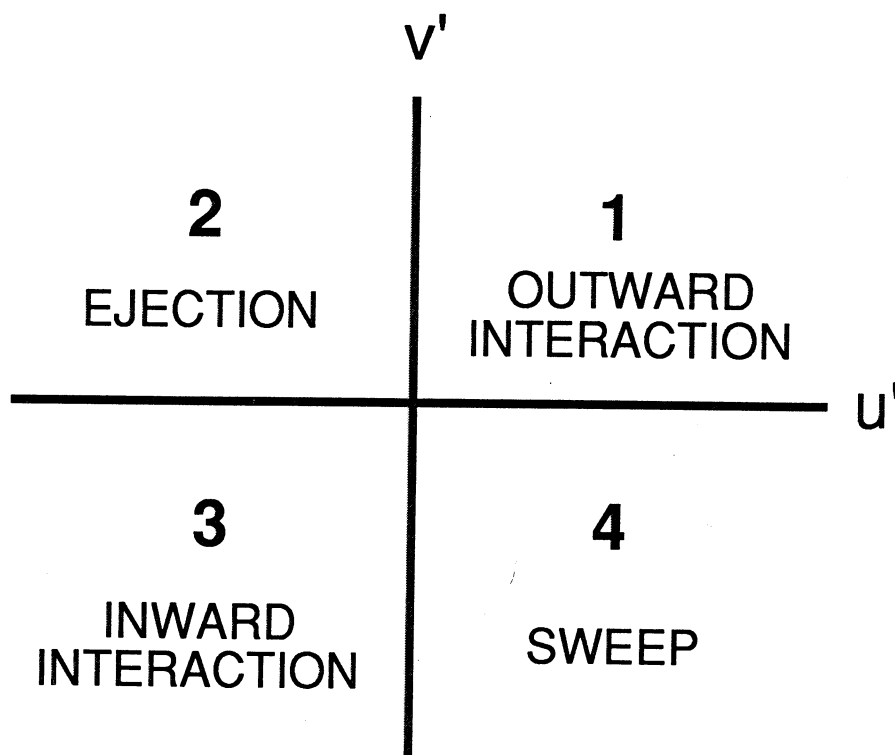


Fig. 4. Quadrants of the u' v' plane.



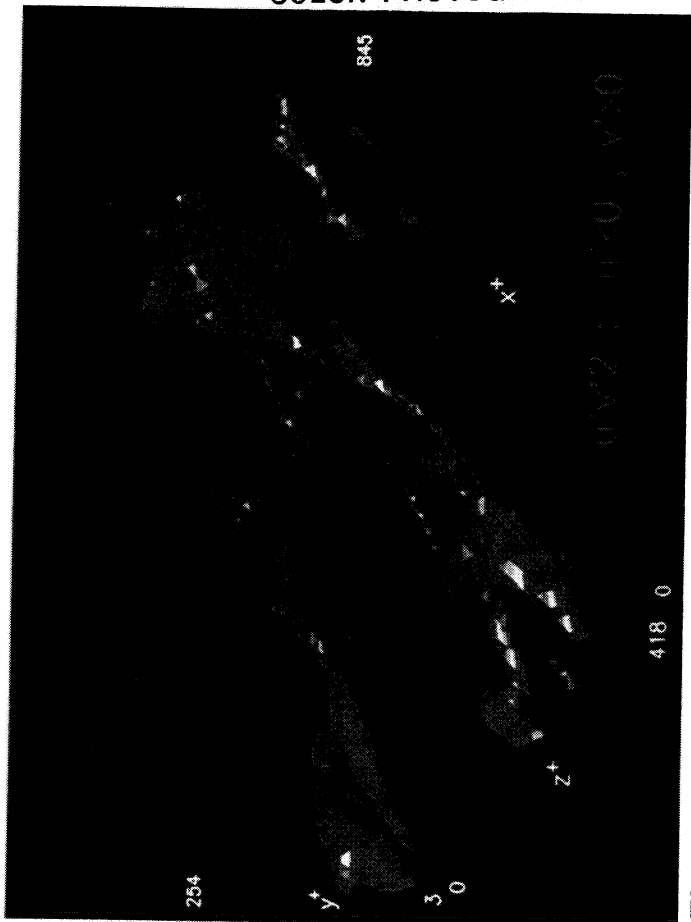


Fig. 7
Fig. 8

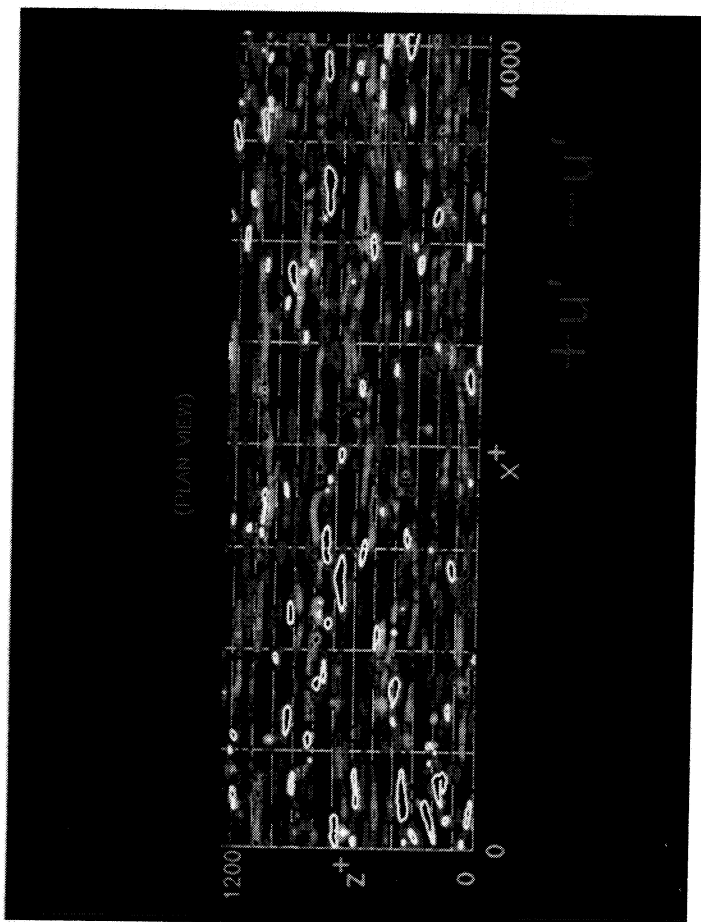
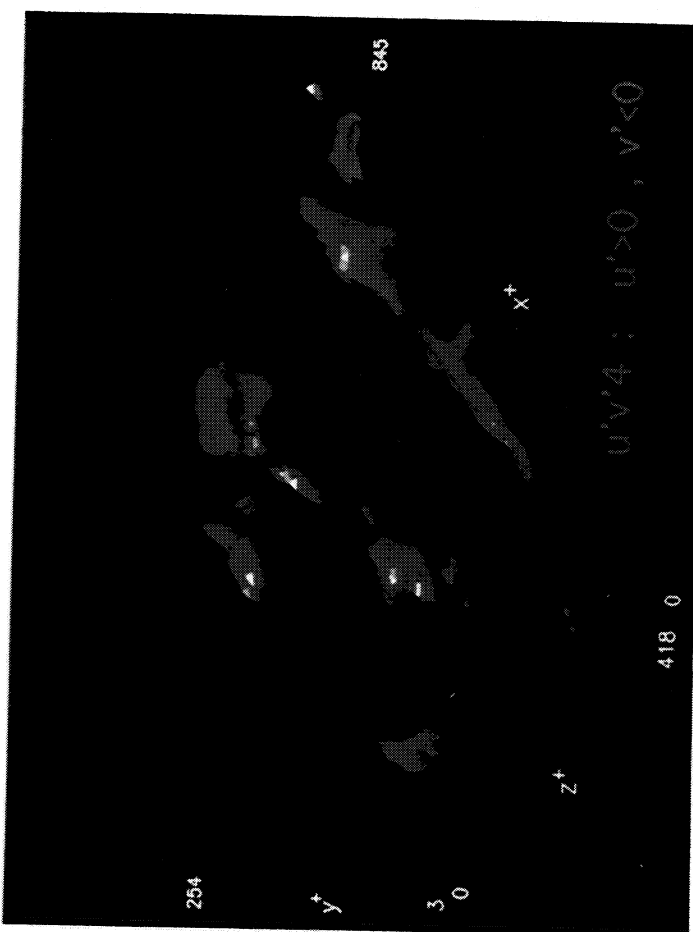
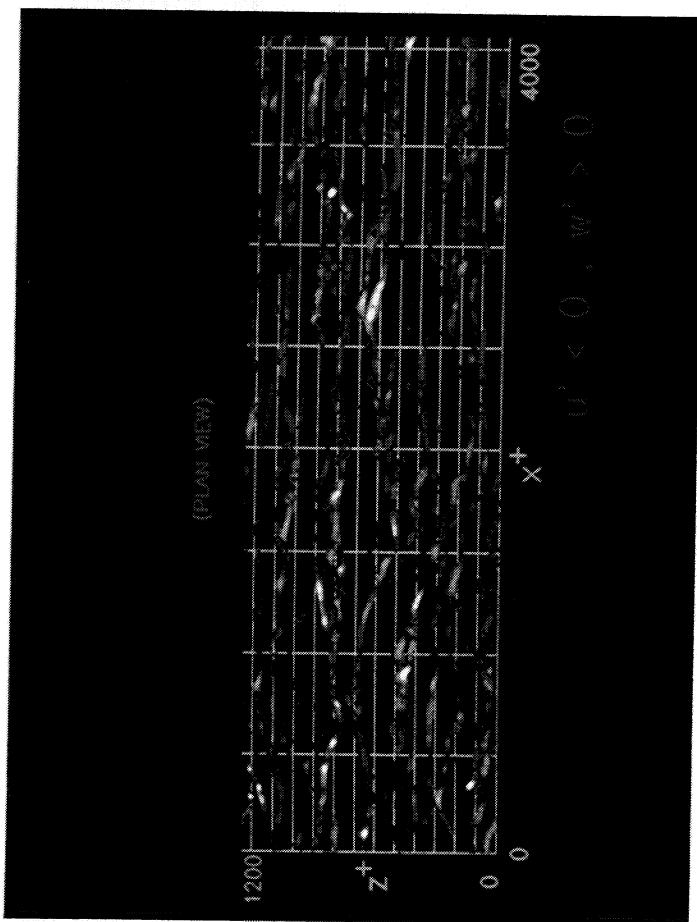


Fig. 5
Fig. 6



PRECEDING PAGE BLANK NOT FILMED

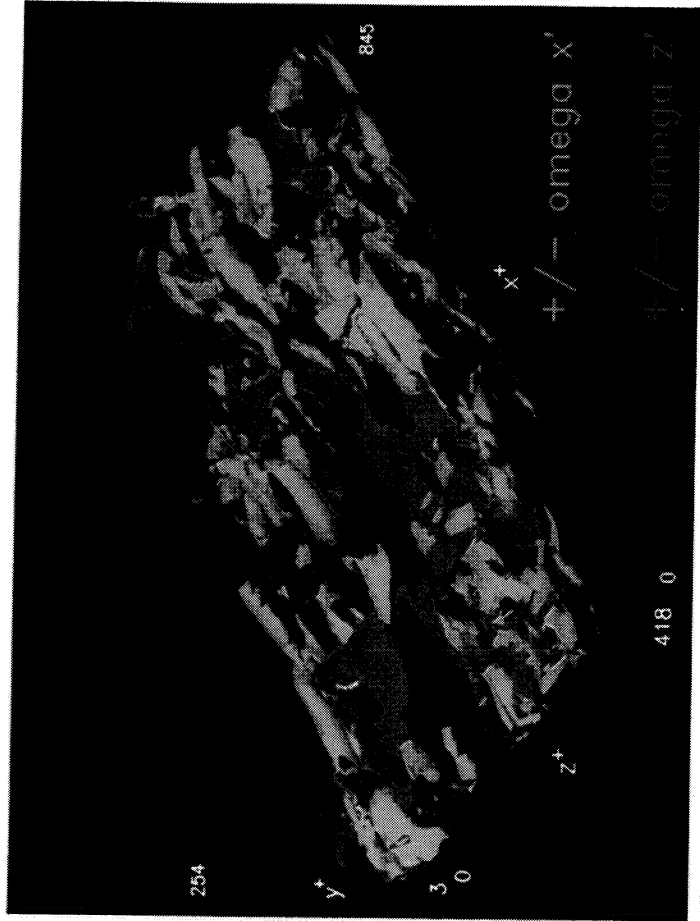


Fig. 11
 Fig. 12

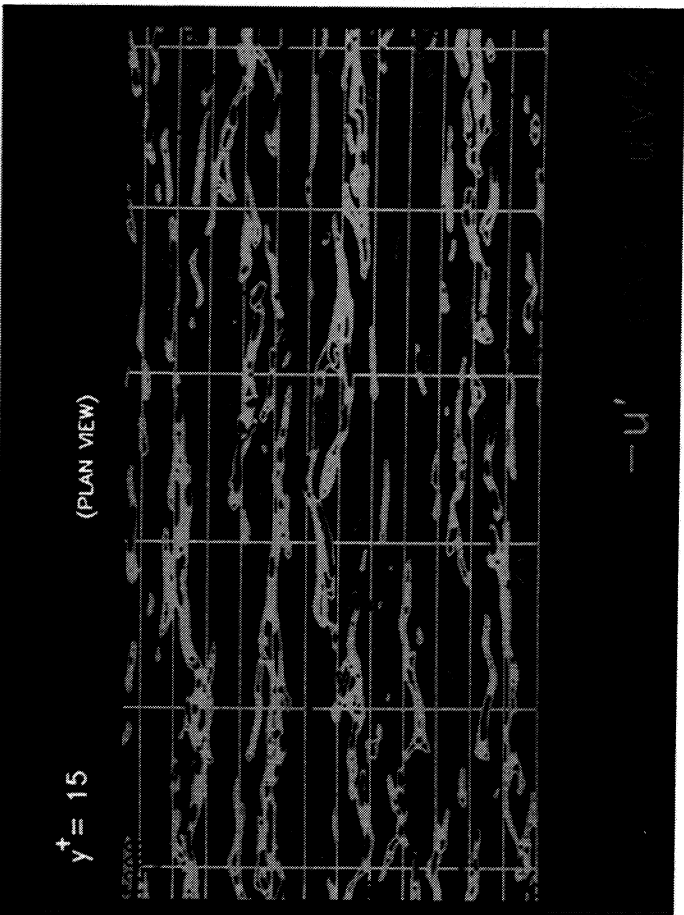
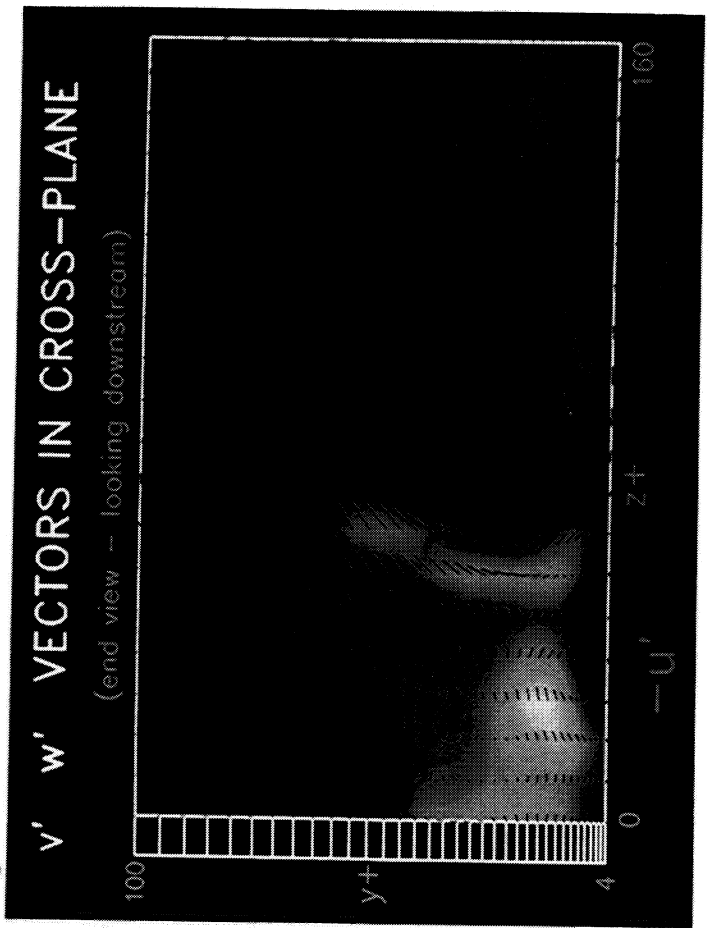
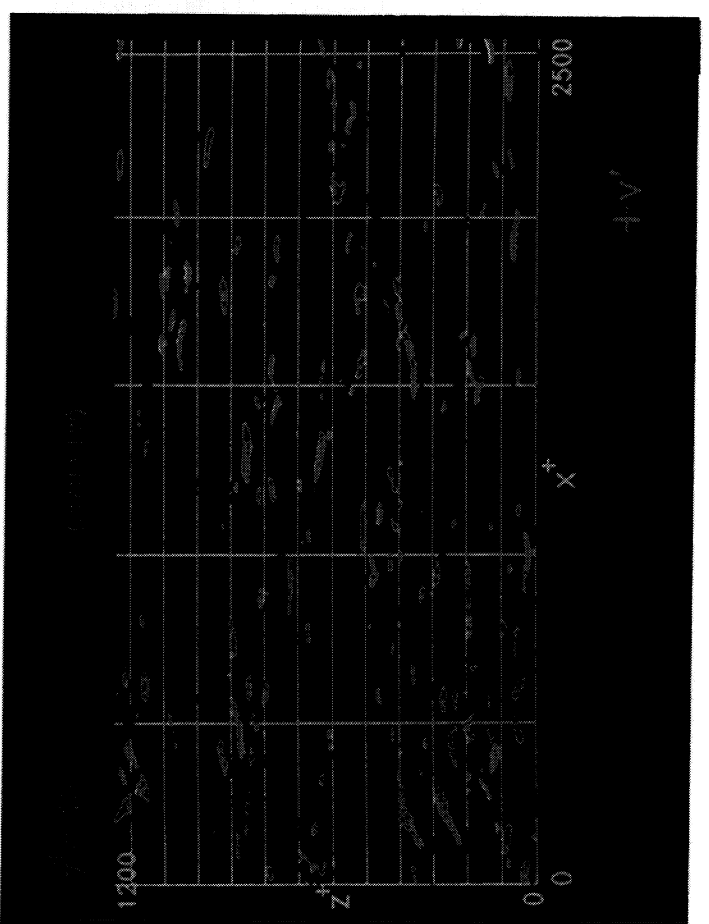


Fig. 9
 Fig. 10



PRECEDING PAGE BLANK NOT FILMED



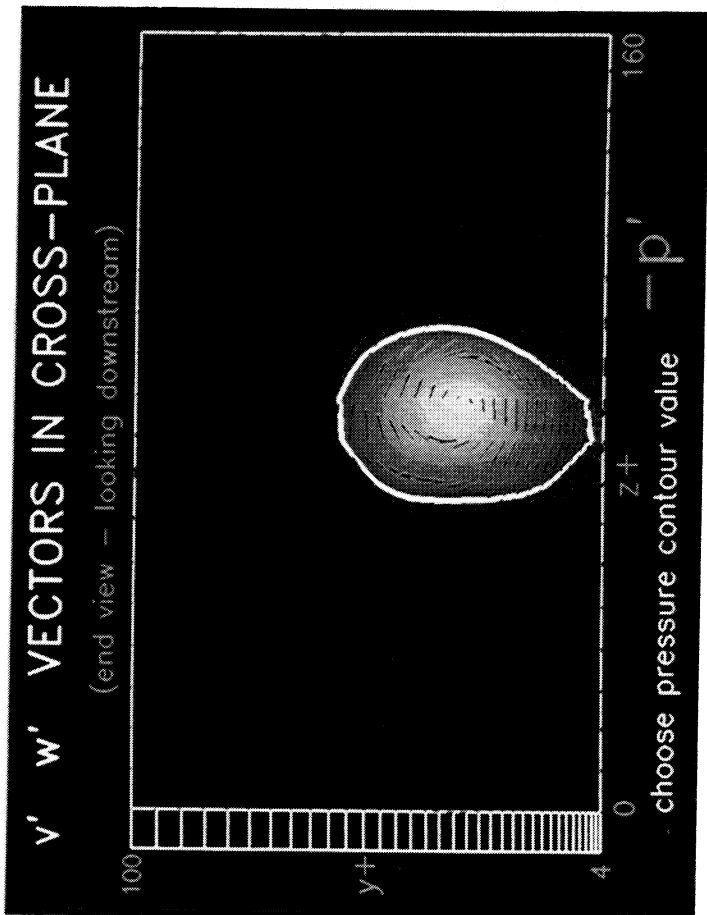


Fig. 13
 Fig. 14

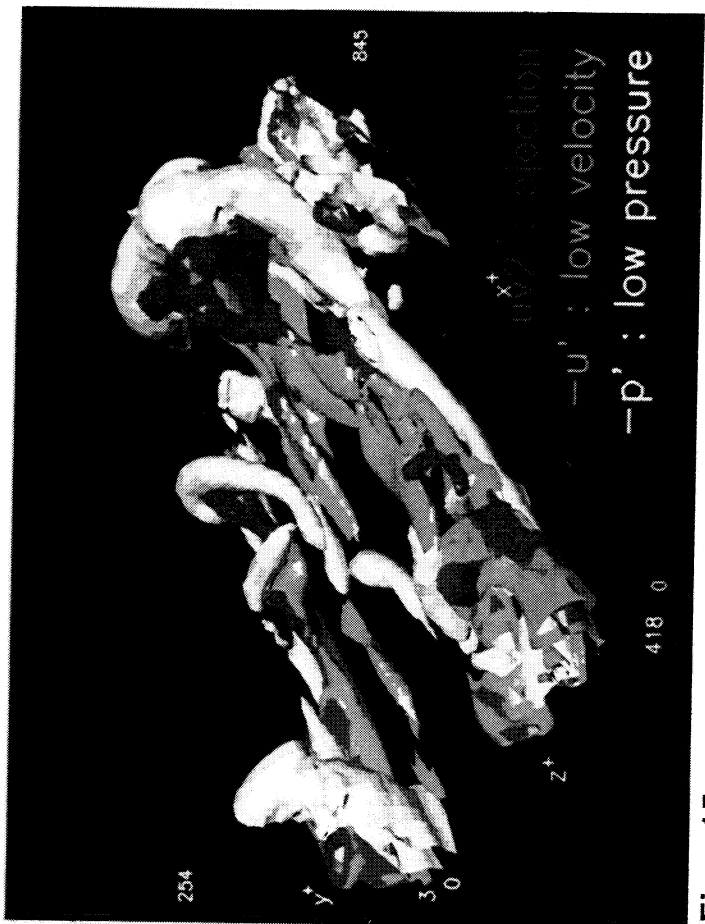
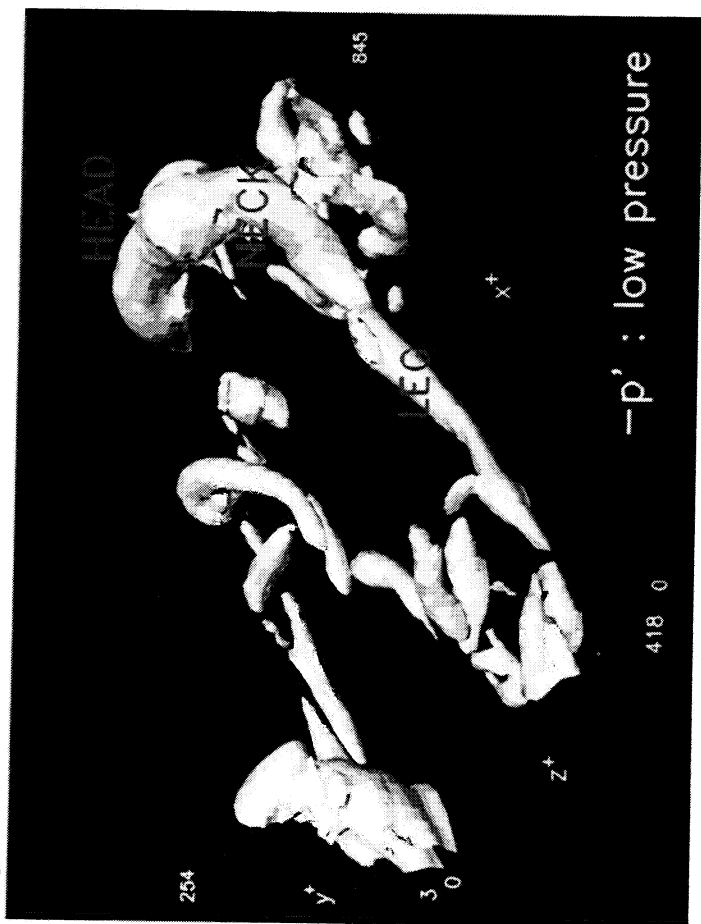
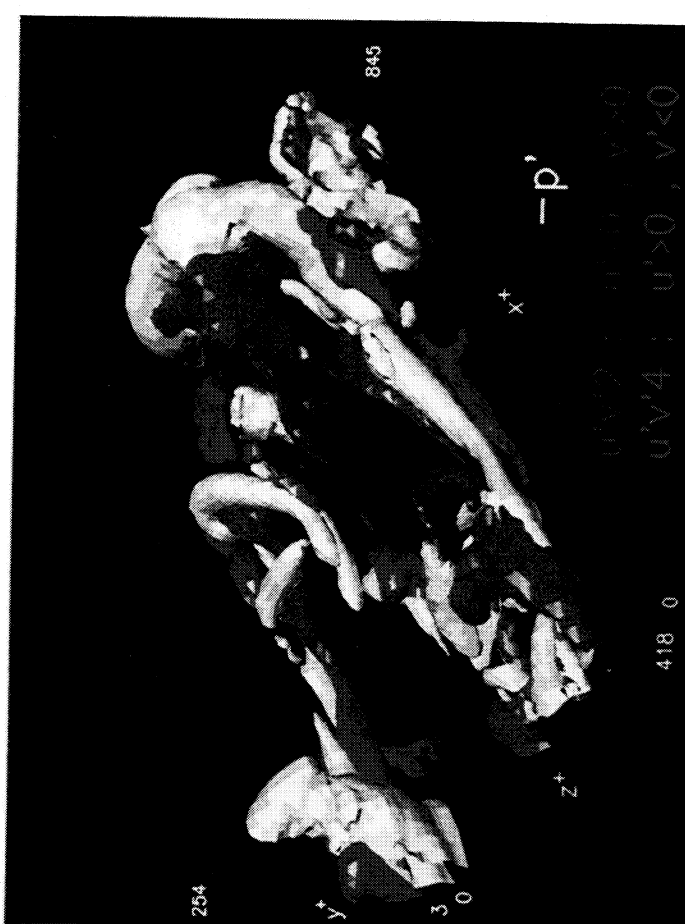


Fig. 15
 Fig. 16





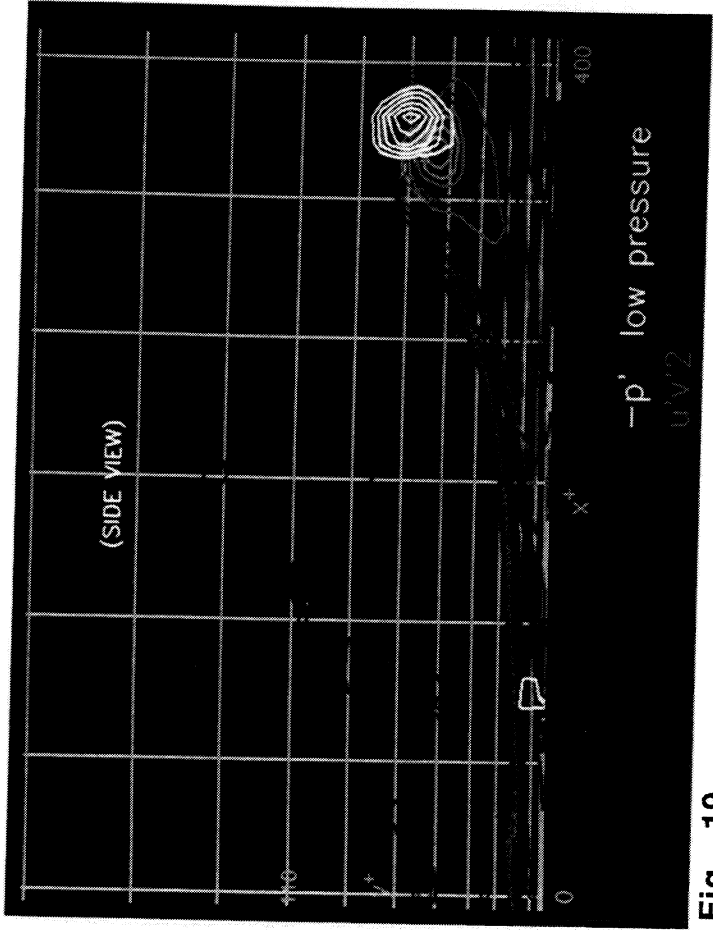


Fig. 19

Fig. 20

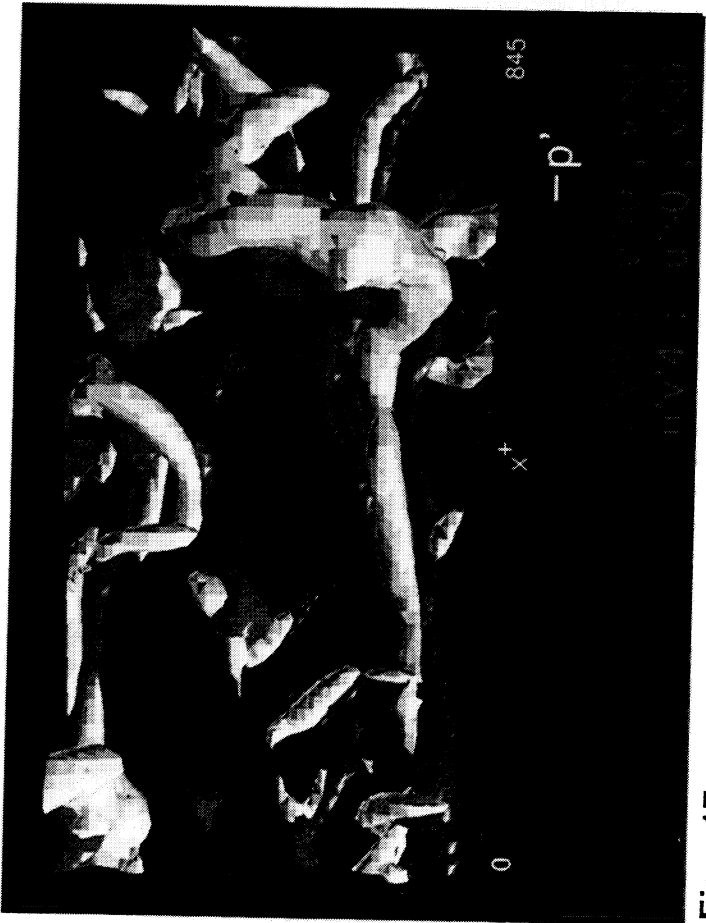
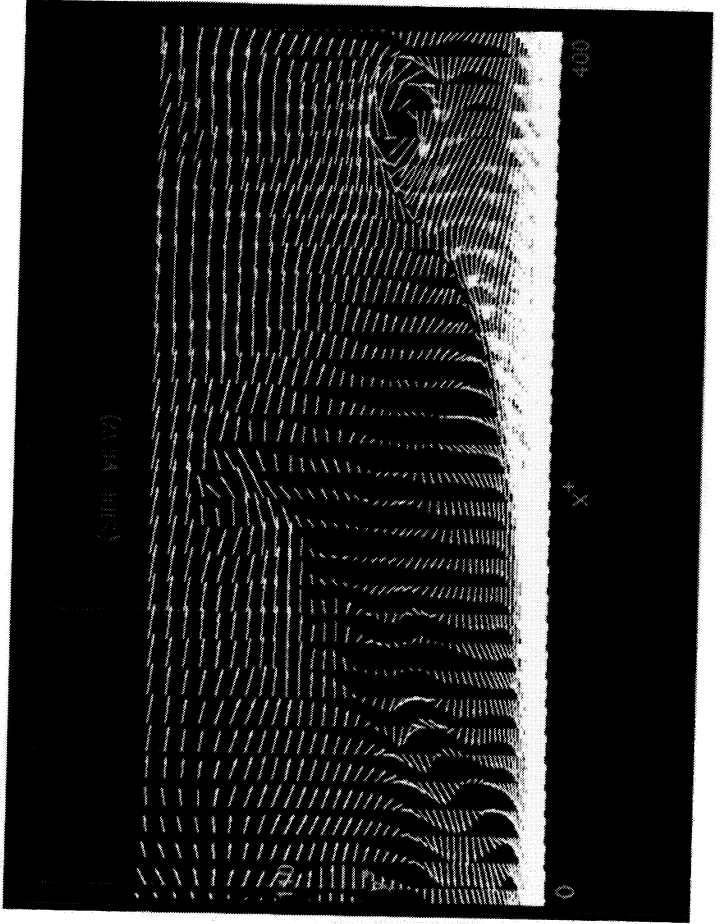
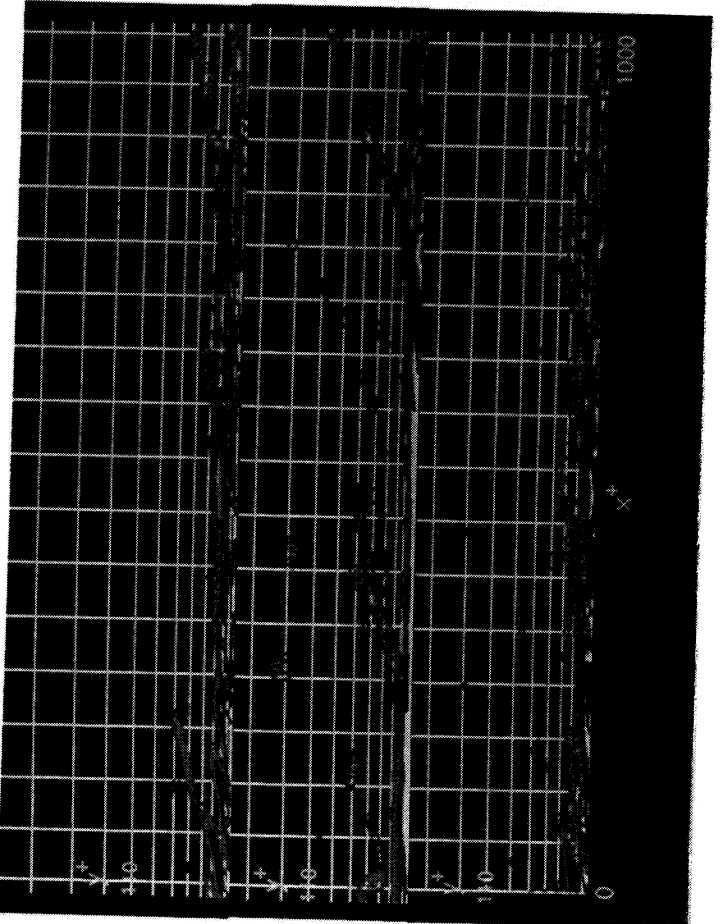


Fig. 17

Fig. 18





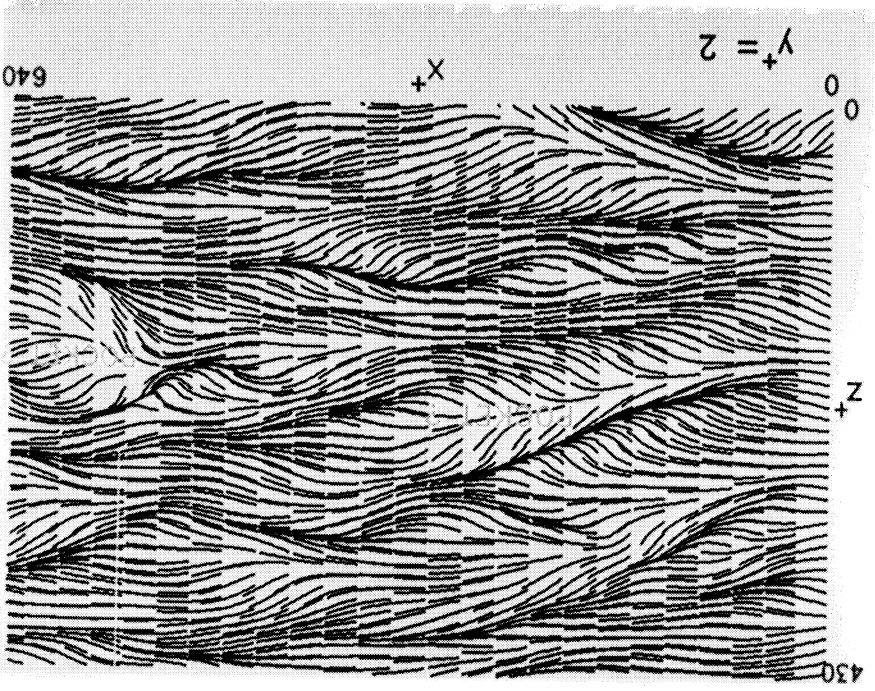


Fig. 23

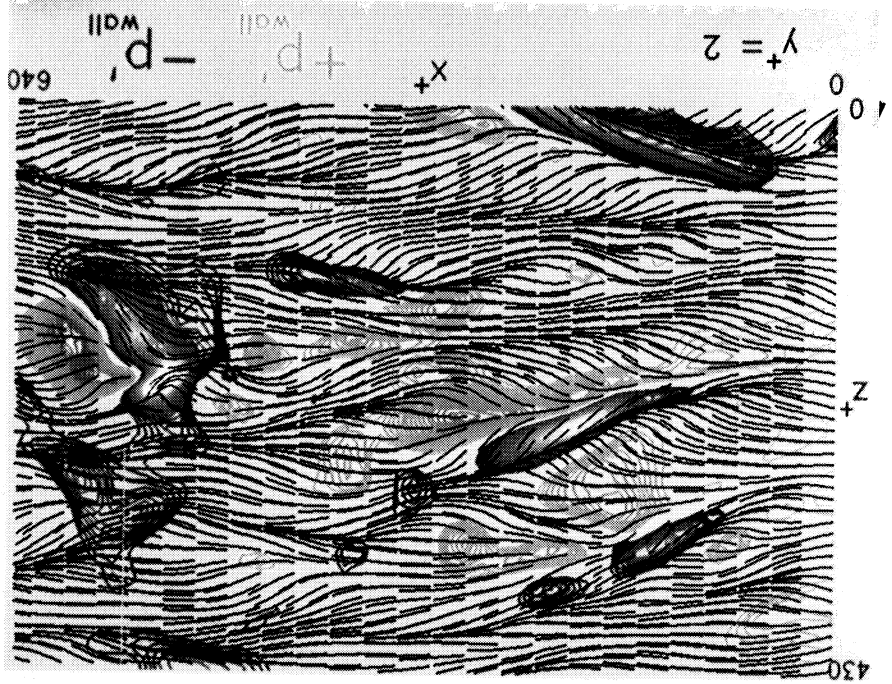


Fig. 24

ORIGINAL PAGE
COLOR PHOTOGRAPH

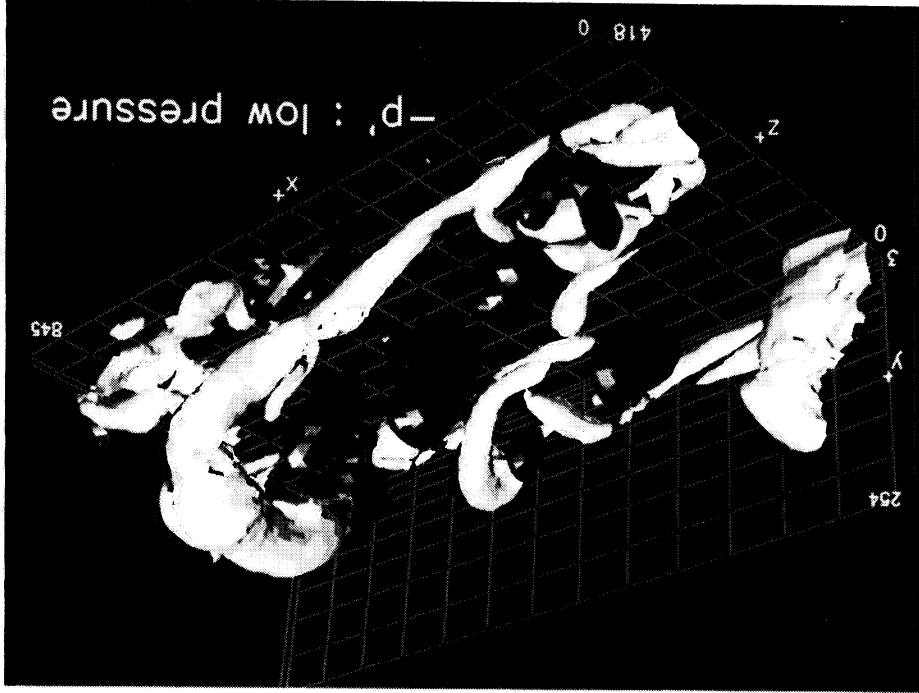


Fig. 21

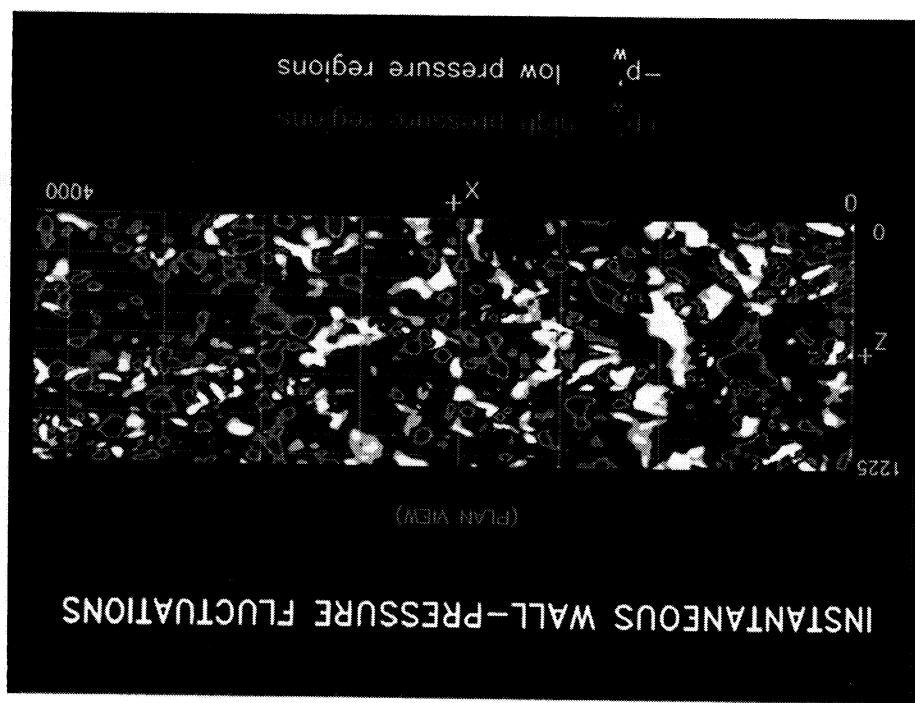


Fig. 22

INSTANTANEOUS WALL-PRESSURE FLUCTUATIONS

(PLAN VIEW)

1950

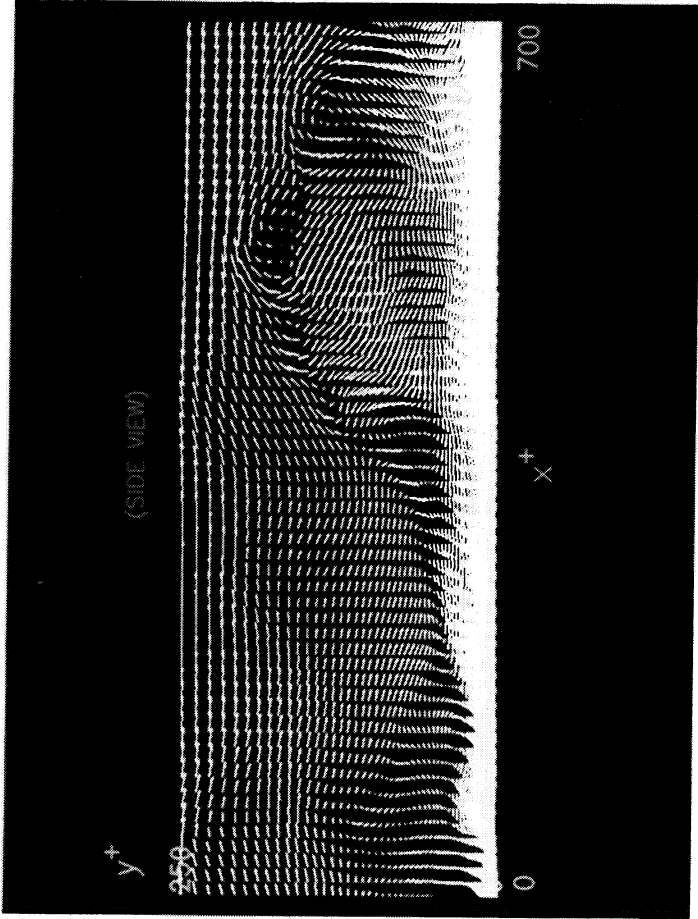


Fig. 27
Fig. 28

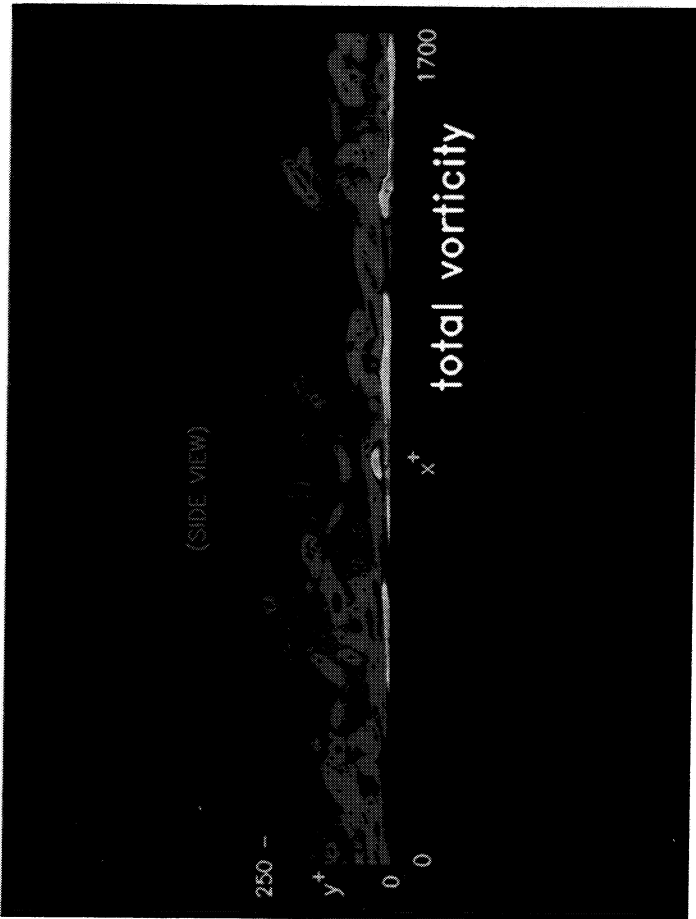
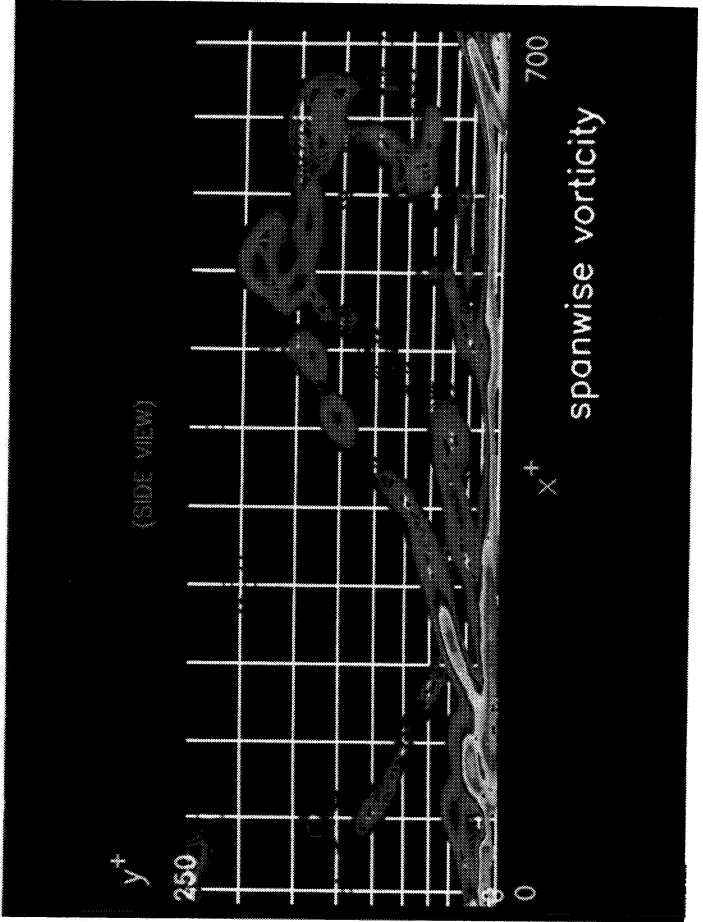
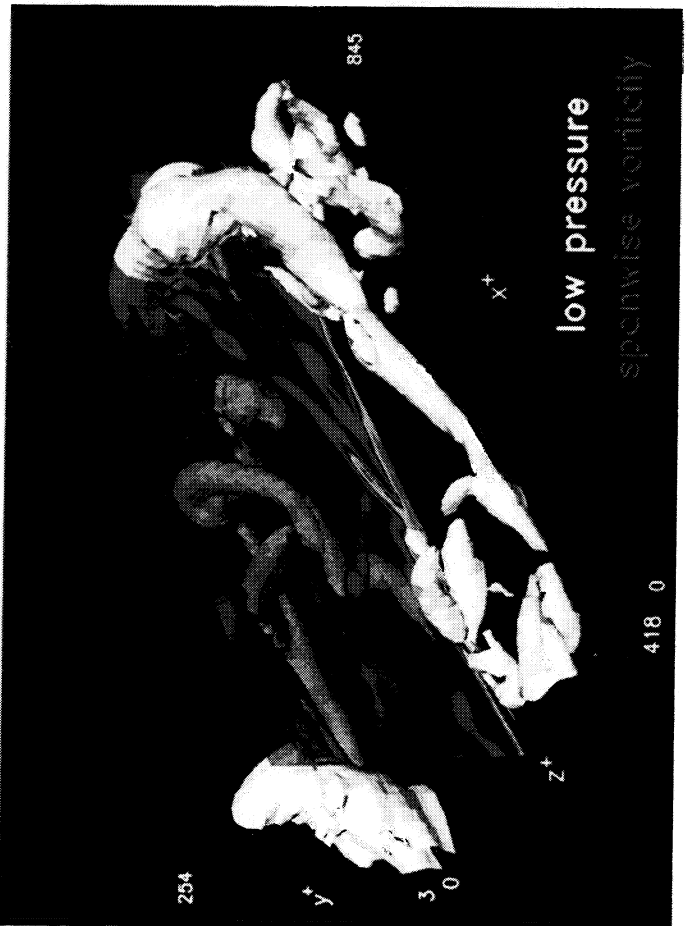


Fig. 25
Fig. 26







Report Documentation Page

1. Report No. NASA TM-102191		2. Government Accession No.		3. Recipient's Catalog No.	
4. Title and Subtitle A Review of Quasi-Coherent Structures in a Numerically Simulated Turbulent Boundary Layer				5. Report Date May 1989	
				6. Performing Organization Code	
7. Author(s) S. K. Robinson, S. J. Kline (Stanford University, Stanford, CA 94305), and P. R. Spalart				8. Performing Organization Report No. A-88294	
				10. Work Unit No. 505-60-11	
9. Performing Organization Name and Address Ames Research Center Moffett Field, CA 94035				11. Contract or Grant No.	
				13. Type of Report and Period Covered Technical Memorandum	
12. Sponsoring Agency Name and Address National Aeronautics and Space Administration Washington, DC 20546-0001				14. Sponsoring Agency Code	
				15. Supplementary Notes Point of Contact: S. K. Robinson, Ames Research Center, MS 229-1, Moffett Field, CA 94035 (415) 694-6220 or FTS 464-6220 Presented as: Quasi-Coherent Structures in the Turbulent Boundary Layer: Part II. Verification and New Information from a Numerically Simulated Flat-Plate Layer at Zoran P. Zaric Memorial International Seminar on Near-Wall Turbulence, May 16-20, 1988, Dubrovnik, Yugoslavia	
16. Abstract <p>This paper presents preliminary results of a comprehensive study of the structural aspects of a numerically simulated number turbulent boundary layer. A direct Navier-Stokes simulation of a flat-plate, zero pressure gradient boundary layer at $Re_\theta = 670$ was used. Most of the known nonrandom, coherent features of turbulent boundary layers are confirmed in the simulation, and several new aspects of their spatial character are reported. The spatial relationships between many of the various structures are described, forming the basis for a more complete kinematical picture of boundary layer physics than has been previously known. In particular, the importance of vortex structures of various forms to the generation of Reynolds shear stress is investigated.</p>					
17. Key Words (Suggested by Author(s)) Turbulence Numerical simulation Boundary layer Coherent structures			18. Distribution Statement Unclassified-Unlimited Subject Category - 34		
19. Security Classif. (of this report) Unclassified		20. Security Classif. (of this page) Unclassified		21. No. of pages 41	22. Price A03

